Geographic variation of mutagenic exposures in kidney cancer genomes

Sergey Senkin[1], Sarah Moody[2], Marcos Díaz-Gay[3,4,5], Behnoush Abedi-Ardekani[1], Thomas Cattiaux[1], Aida Ferreiro-Iglesias[1], Jingwei Wang[2], Stephen Fitzgerald[2], Mariya Kazachkova[3,6,5], Raviteja Vangara[3,4,5], Anh Phuong Le[2], Erik N. Bergstrom[3,4,5], Azhar Khandekar[3,4,5], Burçak Otlu[3,4,5,7], Saamin Cheema[2], Calli Latimer[2], Emily Thomas[2], Joshua Ronald Atkins[8], Karl Smith-Byrne[8], Ricardo Cortez Cardoso Penha[1], Christine Carreira[9], Priscilia Chopard[1], Valérie Gaborieau[1], Pekka Keski-Rahkonen[10], David Jones[2], Jon W. Teague[2], Sophie Ferlicot[11], Mojgan Asgari[12], Surasak Sangkhathat[13], Worapat Attawettayanon[14], Beata Świątkowska[15], Sonata Jarmalaite[16,17], Rasa Sabaliauskaite[16], Tatsuhiro Shibata[18,19], Akihiko Fukagawa[19,20], Dana Mates[21], Viorel Jinga[22], Stefan Rascu[22], Mirjana Mijuskovic[23], Slavisa Savic[24], Sasa Milosavljevic[25], John M.S. Bartlett[26], Monique Albert[27], Larry Phouthavongsy[28], Patricia Ashton-Prolla[29,30], Mariana R. Botton[31], Brasil Silva Neto[32,33], Stephania Martins Bezerra[34], Maria Paula Curado[35], Stênio de Cássio Zequi[36,37,38,39], Rui Manuel Reis[40,41], Eliney Faria[42], Nei Soares Menezes[43], Renata Spagnoli Ferrari[42], Rosamonde E. Banks[44], Naveen S. Vasudev[44], David Zaridze[45], Anush Mukeriya[45], Oxana Shangina[45], Vsevolod Matveev[46], Lenka Foretova[47], Marie Navratilova[47], Ivana Holcatova[48,49], Anna Hornakova[50], Vladimir Janout[51], Mark Purdue[52], Stephen J. Chanock[52], Per Magne Ueland[53], Mattias Johansson[1], James McKay[1], Ghislaine Scelo[54], Estelle Chanudet[55], Laura Humphreys[2], Ana Carolina de Carvalho[1], Sandra Perdomo[1], Ludmil B. Alexandrov[3,4,5], Michael R. Stratton[2], Paul Brennan[1]*

[1]Genomic Epidemiology Branch, International Agency for Research on Cancer (IARC/WHO), Lyon, France, [2]Cancer, Ageing and Somatic Mutation, Wellcome Sanger Institute, Cambridge, UK, [3]Department of Cellular and Molecular Medicine, University of California San Diego, La Jolla, USA, [4]Department of Bioengineering, University of California San Diego, La Jolla, USA, [5]Moores Cancer Center, University of California San Diego, La Jolla,

28 USA, [6]Biomedical Sciences Graduate Program, University of California San Diego, La Jolla,
29 USA, [7]Department of Health Informatics, Graduate School of Informatics, Middle East
30 Technical University, Ankara, Turkey, [8]Cancer Epidemiology Unit, The Nuffield Department
31 of Population Health, University of Oxford, Oxford, UK, [9]Evidence Synthesis and
32 Classification Branch, International Agency for Research on Cancer (IARC/WHO), Lyon,
33 France, [10]Nutrition and Metabolism Branch, International Agency for Research on Cancer
34 (IARC/WHO), Lyon, France, [11]Service d'Anatomie Pathologique, Assistance Publique-
35 Hôpitaux de Paris, Univeristé Paris-Saclay, Le Kremlin-Bicêtre, France, [12]Oncopathology
36 Research Center, Iran University of Medical Sciences, Tehran, Iran, [13]Translational Medicine
37 Research Center, Faculty of Medicine, Prince of Songkla University, Hat Yai, Thailand,
38 [14]Department of Surgery, Urology, Faculty of Medicine, Prince of Songkla University, Hat Yai,
39 Thailand, [15]Department of Environmental Epidemiology, Nofer Institute of Occupational
40 Medicine, Łódź, Poland, [16]Laboratory of Genetic Diagnostic, National Cancer Institute,
41 Vilnius, Lithuania, [17]Department of Botany and Genetics, Institute of Biosciences, Vilnius
42 University, Vilnius, Lithuania, [18]Laboratory of Molecular Medicine, The Institute of Medical
43 Science, The University of Tokyo, Minato-ku, Japan, [19]Division of Cancer Genomics,
44 National Cancer Center Research Institute, Chuo-ku, Japan, [20]Department of Pathology,
45 Graduate School of Medicine, The University of Tokyo, Bunkyo-ku, Japan, [21]Occupational
46 Health and Toxicology, National Center for Environmental Risk Monitoring, National Institute
47 of Public Health, Bucharest, Romania, [22]Urology Department, "Carol Davila" University of
48 Medicine and Pharmacy - "Prof. Dr. Th. Burghele" Clinical Hospital, Bucharest, Romania,
49 [23]Clinic of Nefrology, Faculty of Medicine, Military Medical Academy, Belgrade, Serbia,
50 [24]Department of Urology, University Hospital “Dr D. Misovic” Clinical Center, Belgrade,
51 Serbia, [25]International Organization for Cancer Prevention and Research, Belgrade, Serbia,
52 [26]Cancer Research UK Edinburgh Centre, Institute of Genetics and Cancer, University of
53 Edinburgh, Edinburgh, Scotland, [27]Centre for Biodiversity Genomics, University of Guelph,
54 Guelph, Canada, [28]Ontario Tumour Bank, Ontario Institute for Cancer Research, Toronto,
55 Canada, [29]Experimental Research Center, Genomic Medicine Laboratory, Hospital de

Clínicas de Porto Alegre, Porto Alegre, Brazil, [30]Post-Graduate Program in Genetics and Molecular Biology, Universidade Federal do Rio Grande do Sul, Porto Alegre, Brazil, [31]Diagnostic Laboratory Service, Personalized Medicine, Hospital de Clínicas de Porto Alegre, Porto Alegre, Brazil, [32]Service of Urology, Hospital de Clínicas de Porto Alegre, Porto Alegre, Brazil, [33]Post-Graduate Program in Medicine: Surgical Sciences, Universidade Federal do Rio Grande do Sul, Porto Alegre, Brazil, [34]Department of Anatomic Pathology, A.C. Camargo Cancer Center, São Paulo, Brazil, [35]Department of Epidemiology, A.C. Camargo Cancer Center, São Paulo, Brazil, [36]Department of Urology, A.C. Camargo Cancer Center, São Paulo, Brazil, [37]National Institute for Science and Technology in Oncogenomics and Therapeutic Innovation, A.C. Camargo Cancer Center, São Paulo, Brazil, [38]Latin American Renal Cancer Group – LARCG, São Paulo, Brazil, [39]Department of Surgery, Division of Urology, Sao Paulo Federal University - UNIFESP, São Paulo, Brazil, [40]Molecular Oncology Research Center, Barretos Cancer Hospital, Brazil, [41]Life and Health Sciences Research Institute (ICVS), School of Medicine, Minho University, Braga, Portugal, [42]Department of Urology, Barretos Cancer Hospital, Brazil, [43]Department of Pathology, Barretos Cancer Hospital, Brazil, [44]Leeds Institute of Medical Research at St James's, University of Leeds, Leeds, UK, [45]Clinical Epidemiology, N.N.Blokhin National Medical Research Centre of Oncology, Moscow, Russia, [46]Department of Urology, N.N.Blokhin National Medical Research Centre of Oncology, Moscow, Russia, [47]Department of Cancer Epidemiology and Genetics, Masaryk Memorial Cancer Institute, Brno, Czech Republic, [48]Institute of Public Health & Preventive Medicine, 2nd Faculty of Medicine, Charles University, Prague, Czech Republic, [49]Department of Oncology, 2nd Faculty of Medicine, Charles University and Motol University Hospital, Prague, Czech Republic, [50]Institute of Hygiene & Epidemiology, 1nd Faculty of Medicine, Charles University, Prague, Czech Republic, [51]Faculty of Health Sciences, Palacky University, Olomouc, Czech Republic, [52]Division of Cancer Epidemiology and Genetics, National Cancer Institute, Rockville, USA, [53]Bevital AS, Bergen, Norway, [54]Observational & Pragmatic Research Institute Pte Ltd,

Singapore, Singapore, [55]Department of Pathology, Radboud University Medical Centre, Nijmegen, Netherlands

These authors contributed equally: Sergey Senkin, Sarah Moody

* Corresponding author: Paul Brennan

ABSTRACT

International differences in the incidence of many cancer types indicate the existence of carcinogen exposures which make a substantial contribution to cancer burden, vary geographically, and have underlying agents thus far unidentified by conventional epidemiology[1]. This pertains to clear cell renal cell carcinomas (ccRCC), for which obesity, hypertension, and tobacco smoking are risk factors but do not explain its geographical variation in incidence[2]. Some carcinogens generate somatic mutations and past exposures can be inferred from the patterns of mutations found in cancer genomes. Therefore, we sequenced the whole genomes of 962 ccRCC from 11 countries of varying incidence. Somatic mutation profiles differed between countries. In Romania, Serbia and Thailand, mutational signatures likely caused by extracts of Aristolochia plants were present in most cases and rare elsewhere. In Japan, a mutational signature of unknown cause was found in >70% cases and <2% elsewhere. Another mutational signature of unknown cause was ubiquitous and associated with kidney cancer incidence rates (p-value$<6 \times 10^{-18}$), with higher numbers of mutations in countries with higher risk. Known signatures of tobacco smoking correlated with tobacco consumption, but no signature was associated with obesity or hypertension suggesting non-mutagenic mechanisms of action underlying these risk factors. The results indicate the existence of multiple, widespread, geographically variable mutagenic exposures to known and unknown agents, which may contribute to the incidence of kidney cancer.

INTRODUCTION

The incidence rates of most adult cancers vary substantially between geographical regions and many such differences are unexplained by known risk factors[1]. Together with unexplained trends in incidence over time, this indicates the likely presence of unknown environmental or lifestyle causes for many cancer types[1]. Kidney cancer, for example, has particularly high incidence rates in Central and Northern Europe, notably in the Czech Republic and Lithuania, and has shown increasing incidence in high income countries in recent decades (**Fig. 1**)[2]. Most kidney cancers are clear cell renal cell carcinomas (ccRCC)[3] for which obesity, hypertension and tobacco smoking are known risk factors[2]. However, these account for <50% of the global ccRCC burden and do not explain geographical or temporal incidence trends. Recently, evidence has also emerged of increased risk associated with environmental exposure to per- and polyfluoroalkyl substances (PFAS)[3], industrial chemicals used in a wide range of consumer and industrial products.

Characterization of mutational signatures within cancer genomes[4] is an approach complementary to conventional epidemiology for investigating unknown causes of cancer. Most cancers contain thousands of somatic mutations that have occurred over the lifetime of the individual. These can be caused by endogenous cellular processes, such as imperfect DNA replication and repair, or by exposure to exogenous environmental or lifestyle mutagens such as ultraviolet radiation in sunlight and compounds in cigarette smoke. Mutational signatures are the patterns of somatic mutation imprinted on genomes by individual mutational processes. Analysis of thousands of cancer genome sequences from most cancer types has established a set of reference mutational signatures including 71 single base substitution (SBS) or doublet base substitution (DBS) signatures, and 18 small insertion and deletion (ID) signatures[5]. A possible etiology has been suggested for 47 SBS/DBS signatures and nine ID signatures.

Previous ccRCC genome sequencing studies have included relatively modest numbers of individuals from a small number of countries with limited variation in ccRCC incidence[6–10] and have not comprehensively examined associations between ccRCC risk factors and mutational signatures. To detect the activity of unknown carcinogens involved in ccRCC development and to investigate the mechanisms of action of known risk factors, we generated and analyzed epidemiological and whole genome sequencing data from a large international series of ccRCC[11].

RESULTS

A total of 962 ccRCC cases from 11 countries in four continents were studied, encompassing: Czech Republic (*n*=259), Russia (*n*=216), United Kingdom (*n*=115), Brazil (*n*=96), Canada (*n*=73), Serbia (*n*=69), Romania (*n*=64), Japan (*n*=36), Lithuania (*n*=16), Poland (*n*=13), and Thailand (*n*=5; **Fig. 1**; **Table 1**; **Methods**). These encompass a broad range of ccRCC incidence, from the highest global age-standardized rates (ASRs) of Lithuania and Czech Republic (ASRs of 14.5 and 14.4/100,000 respectively) to the relatively low rates of Brazil and Thailand (ASRs of 4.5 and 1.8/100,000 respectively)[12]. Epidemiological questionnaire data were available on sex, age at diagnosis, and important risk factors including body mass index (BMI), hypertension, and tobacco smoking (**Table 1**). DNAs from ccRCCs and blood from the same individuals were extracted and whole genome sequenced to average coverage of 54-fold and 31-fold, respectively.

Somatic mutation burdens in the 962 ccRCC genomes ranged from 803 to 45,376 (median 5,093) for single base substitutions (SBS), 2 to 240 (median 53) for doublet base substitutions (DBS), and 10 to 14,770 (median 695) for small insertions and deletions (**Supplementary Table 1**). The average burden in all these three mutation types differed between the 11 countries (p-value$<2 \times 10^{-23}$, p-value $<2 \times 10^{-14}$, p-value $<6 \times 10^{-14}$, for SBSs, DBSs, and IDs, respectively). In particular, the burden of all mutation types was elevated in Romania compared

to other countries (**Extended Data Fig. 1**). Principal Component Analysis (PCA) performed on the proportions of the six primary SBS mutation classes (C>A, C>G, C>T, T>A, T>C, T>G) in each sample identified a distinct cluster of mainly Romanian and Serbian cases and a further cluster of mainly Japanese cases (**Extended Data Fig. 2**). The results, therefore, clearly demonstrate geographical variation of somatic mutation loads and patterns in ccRCC.

To investigate the mutational processes contributing to the geographical variation in mutation burdens we extracted mutational signatures and estimated the contribution of each signature to each ccRCC genome. Ten signatures with strong similarity to a reference signature in the Catalogue of Somatic Mutations in Cancer (COSMIC) database were extracted: SBS1, due to deamination of 5-methylcytosine[13]; SBS2 and SBS13, due to cytosine deamination by Apolipoprotein B mRNA-editing enzyme, catalytic polypeptide-like (APOBEC) DNA editing enzymes[13]; SBS4, due to tobacco smoke mutagens[14]; SBS5, due to an endogenous mutational process in which mutations accumulate with age[14]; SBS12, of unknown cause; SBS18, due to DNA damage by reactive oxygen species[14]; SBS21 and SBS44, due to defective DNA mismatch repair[14,15]; and SBS22, due to Aristolochic acid exposure[16,17].

Five further SBS signatures were identified but could not be well described by the COSMIC catalogue (**Fig. 2**; **Supplementary Table 5**). SBS40a, SBS40b and SBS40c were present in most ccRCC accounting for, on average, ~30%, ~20%, and ~3% of mutations respectively (**Fig. 2b**). Combined, they closely resemble the previously reported SBS40 (0.97 cosine similarity), suggesting that the large number of ccRCC whole genomes analyzed here provides the power to separate the constituent component signatures of SBS40. SBS40 was previously reported frequently, and at high levels, in kidney cancer, but also in other cancers, and is of unknown etiology. Like the composite SBS40, SBS40a is present in multiple cancer types. However, SBS40b and SBS40c are largely restricted to ccRCC (**Supplementary Note 1**). SBS_H was found in a single case and SBS_I is related to Aristolochic acid exposure (see

191 below; SBS_I has been renamed as SBS22b). Analysis of all other types of mutational
192 signatures is presented in Supplementary results.
193
194 The mutation burdens of multiple SBS mutational signatures varied between the 11 countries.
195 SBS22 is thought to be caused by Aristolochic acids, mutagenic derivatives of plants of the
196 Aristolochia genus which are carcinogenic and also cause Balkan endemic nephropathy
197 (BEN), a kidney disease prevalent in areas adjacent to the Danube in Southeastern Europe[18].
198 SBS22 has previously been found in ccRCC, other urothelial tract cancers, and hepatocellular
199 carcinomas from Romania[6,19] and various countries in East and South-East Asia[16,17,20]. In this
200 study, SBS22 was present in high proportions of ccRCC from Romania (45/64, 70%), Serbia
201 (16/69, 23%), and Thailand (3/5, 60%), often with very high mutation burdens. The presence
202 of SBS22 was strongly correlated with that of new signatures SBS_I, DBS_D, and ID_C
203 (**Extended Data Fig. 3-5**) which are, therefore, also probably due to Aristolochic acid
204 exposure. SBS_I, like SBS22, is composed predominantly of T>A mutations. The signature
205 identified previously as SBS22, has therefore been renamed SBS22a, and SBS_I has been
206 named SBS22b. The two signatures may be due to different subsets of Aristolochic acids,
207 and/or to different metabolites, which induce slightly different mutational patterns. All these
208 signatures exhibited their highest mutation loads away from recognized BEN zones (**Fig. 3**)
209 indicating that a substantial proportion of the population over a wide geographical area of
210 Eastern Europe has been subject to mutagenesis due to Aristolochic acid exposure. The
211 sources of this exposure are uncertain.
212
213 SBS12 was present in 72% of Japanese and 2% of non-Japanese ccRCC (p-
214 value=4.7×10^{-78}) (**Extended Data Fig. 6h**). Compared to the mutation burdens imposed by
215 Aristolochic acid in ccRCC, SBS12 contributed modest mutation loads. SBS12 is composed
216 predominantly of T>C substitutions and exhibits strong transcriptional strand bias with more
217 T>C mutations on the transcribed than untranscribed strands of protein coding genes.
218 Transcriptional strand bias is typically caused by activity of transcription-coupled nucleotide

219 excision repair acting on bulky DNA adducts due to exogenous mutagenic exposures such as
220 tobacco smoke chemicals[14], ultraviolet light[14], Aristolochic acids[16], and aflatoxins[21]. Assuming
221 that transcription-coupled repair of DNA adducts is responsible for the SBS12 strand bias, the
222 adducts are likely on adenine. SBS12 was previously reported in hepatocellular carcinomas[5,14]
223 and additional analysis of existing datasets revealed strong SBS12 enrichment in
224 hepatocellular carcinomas from Japan when compared to other countries (p-value=3.8×10^{-15};
225 **Supplementary Note**). The results, therefore, indicate that exposure to an agent contributing
226 SBS12 mutations to kidney and liver cancer is common in Japan and rare elsewhere. The
227 agent responsible for SBS12 is unknown. Although population-specific endogenous production
228 of the mutagen cannot be excluded, the precedents provided by other mutational signatures
229 with strong transcriptional strand bias suggest that it is likely of exogenous origin. A
230 polymorphism in aldehyde dehydrogenase 2 known to impair metabolism of alcohol to
231 aldehydes and common in Japan did not associate with levels of SBS12 (although power is
232 limited due to the relatively small number of Japanese cases).
233
234 SBS40a, SBS40b, and SBS40c were present in ccRCC from all 11 countries. The country-
235 specific average mutation burdens of SBS40a and SBS40b positively associated with country-
236 specific ASRs of kidney cancer incidence (p-value=0.0022 and p-value=5.1×10^{-18},
237 respectively; **Extended Data Fig. 7a**; **Fig. 4a**), with the highest mutation loads in the Czech
238 Republic and Lithuania. Indeed, when excluding the outlier effect of Romania and Serbia,
239 SBS40b was largely responsible for association of country-specific average total SBS burdens
240 with kidney cancer ASR (p-value=6×10^{-5}; **Extended Data Fig. 8a)**. Kidney cancer incidence
241 rates also vary between the regions of the Czech Republic and SBS40b mutation burdens
242 differed significantly between these (p-value=0.011; **Fig 4b,c**), with the highest attribution in
243 the highest risk region. SBS40b exhibits modest transcriptional strand bias and, assuming that
244 transcription-coupled repair of DNA adducts is responsible, the adducts underlying SBS40b
245 are likely on pyrimidines. Insertion and deletion (indel) signatures ID5 and ID8, which together
246 contributed ~60% of the indel mutation burden on average, were also strongly associated with

country-specific kidney cancer ASR (p-value=1.3×10^{-10} and p-value=6.2×10^{-9}, respectively, **Extended Data Fig. 7b,c**). Signatures ID5 and ID8 correlated with each other (0.78), as well as with SBS40b (0.81 and 0.74, respectively) indicating that they likely all constitute products of the same underlying mutational process. Thus, the burdens of the full complement of mutation types generated by this mutational process correlate with age-adjusted kidney cancer incidence rates.

To investigate potential mutagenic agents underlying these geographically variable signatures, an untargeted metabolomics screen of plasma was conducted on 901 individuals in the study, from all countries except Japan (**Methods**). 2,392 metabolite features were obtained, including 944 independent peaks ($r<0.85$). Three features were associated with SBS4 (**Supplementary Table 13**), with two identified as hydroxycotinine (p-value=2.9×10^{-9}) and cotinine (p-value=1.9×10^{-5}), two major metabolites of nicotine[22]. Eight features were associated with SBS40b (**Supplementary Table 13**). One feature was identified as N,N,N-trimethyl-L-alanyl-L-proline betaine (TMAP; p-value=1.2×10^{-5}), increased levels of which correlate strongly with reduced kidney function[23]. Other established measures of kidney function, including cystatin C and creatinine, were correlated with TMAP (p-value = 2.5×10^{-30} and 1.7×10^{-69}, respectively) and also showed evidence of positive association with SBS40b (p-value=0.023 and 0.058, respectively). Thus, exposure to the mutagenic agent responsible for SBS40b is associated with reduced kidney function. No recognized metabolome features were significantly associated with any other signatures.

A total of 1913 “driver” mutations were found in 136 genes including *VHL*, *PBRM1*, *SETD2* and *BAP1*, the known frequently mutated cancer genes in ccRCC (Methods) (**Fig. 5a**)[10,24]. The frequencies of mutations in these genes were consistent across countries (**Fig. 5b**). The spectrum of all driver mutations in ccRCC with Aristolochic acid exposure (**Methods**) was enriched in T>A mutations compared to non-exposed cases (25% vs 13%, p-value=0.0062, **Fig. 5c,d**) with similar enrichment specifically in VHL mutations (30% vs 16%; **Fig. 5e,f**), and

in the whole exome (27% in exposed compared to 12% in unexposed cases). Thus genome-wide Aristolochic acid mutagenesis has contributed in a proportionate fashion to generation of driver mutations in Aristolochic acid-exposed ccRCC. SBS12 did not show statistically significant enrichment in drivers in exposed cases, possibly due to the smaller numbers of SBS12 exposed cases and the lower mutation burden conferred. SBS40b also did not show statistically significant enrichment probably due to the ubiquitous exposure and its relatively flat and featureless mutation profile.

Exogenous mutagenic exposures that ultimately cause cancer may be present during the early stages of evolution of cancer clones. To time mutagenic exposures, the contribution of each mutational signature to mutations in the primary clone (relatively early) and to mutations in subclones (relatively late) were estimated[25,26] (**Methods**). All signatures of the putative exogenous mutagenic exposures observed in ccRCC were present at relatively early stages of cancer development, consistent with exposures to normal cells. SBS12, SBS22b, and SBS40b showed higher activities in main clones compared to subclones (q-value=0.04, q-value=0.02, q-value=2.3×10^{-5}, respectively) (**Extended Data Fig. 9**) and SBS22a showed no significant difference[16,17]. By contrast, signatures due to endogenous mutational processes including APOBEC DNA editing (SBS13) and oxidative damage (SBS18), were enriched in subclones (q-value=1.6×10^{-4}, q-value=3.2×10^{-7}, respectively).

Established or suspected risk factors for ccRCC include age, tobacco smoking, obesity, hypertension, diabetes, and environmental exposure to PFAS compounds[3]. Total SBS, DBS, and ID mutation burdens associated with age, as did SBS1, SBS4, SBS5, SBS40a, SBS40b, SBS22a, SBS22b, DBS2, ID1, ID5, and ID8. Total SBS (p-value=2.8×10^{-5}), DBS (p-value=3.5×10^{-3}) and ID (p-value=1.1×10^{-4}) mutation burdens also associated with sex, with males having higher mutation burdens than females, and with SBS40b showing a similar association (p-value=7.6×10^{-5}). Associations with tobacco smoking were observed for SBS4 (p-value=5.5×10^{-6}) and DBS2 (p-value=2.3×10^{-7}), both known to be caused by tobacco

carcinogens[27,28], but associations of particular mutational signatures with other ccRCC risk factors were not observed (**Supplementary Tables 8-9**). To complement this analysis of observational data, associations between polygenic risk scores for known ccRCC risk factors and mutational signatures[29,30] were examined (**Methods**). Consistent with the observational data, no associations were found between genetically inferred risk factors and mutational signatures except for tobacco smoking and DBS2 (p-value=0.008; **Supplementary Table 10**).

DISCUSSION

Somatic mutations in the genomes of 962 ccRCC patients from 11 countries indicate the existence of multiple, widespread mutational processes exhibiting substantial geographical variation in their contributions to ccRCC mutation loads. The results contrast with those from 552 esophageal squamous carcinomas from eight countries with widely different esophageal carcinoma incidence rates in which geographical differences in mutation burdens or signatures were not observed[31]. Together the studies implicate both geographically variable mutagenic and non-mutagenic carcinogenic exposures contributing to global cancer incidence. Indeed, the presence of mutational signatures associated with tobacco smoking but absence of signatures associated with other known ccRCC risk factors, such as obesity and hypertension, suggests that the latter may be mediated by non-mutagenic processes and, therefore, that both classes of carcinogen contribute to the development of ccRCC.

The existence, identity, and carcinogenic effect of some of the agents underlying these mutational processes are known. Aristolochic acids are believed to cause SBS22a/b and its associated signatures and this study suggests that the geographical extent and proportion of the population acquiring mutations in Eastern Europe may be greater than previously anticipated. The sources of the Aristolochic acid exposure, the manner by which they are ingested and whether the exposure continues today are uncertain and further definition of the source and extent of this exposure is required in order to provide a foundation for public health action.

The existence of the mutagenic exposures underlying SBS12 and SBS40b were not previously suspected, and their causative agents are unknown. Based on current information, the exposure causing SBS12 is restricted to Japan. However, larger studies are now indicated to explore the geographical extent of exposure in Japan and neighboring countries, and the proportions of their populations developing mutations. In the first instance this will be achievable by further sequencing of kidney and hepatocellular cancer genomes. However, studies of normal tissues, using recently reported sequencing methods allowing detection of somatic mutations in normal cells[32], and particularly relatively accessible ones such as cells in urine that can be prospectively collected, may enable large population-based studies providing better characterization of the exposure and its consequences.

In contrast to Aristolochic acid and the agent causing SBS12, the exposure underlying SBS40b appears to be globally ubiquitous. It predominantly causes mutations in ccRCC, with much lower burdens in other cancer types, and generates mutation loads correlating strongly with age and sex. There are few clues as to its origin or nature.

The incidence rates of ccRCC vary ~eightfold across the eleven countries from which ccRCCs were sequenced. A strong positive correlation (p-value=5.5×10^{-18}) was found between the average mutation loads attributable to SBS40b in each country (and also those of ID5 and ID8 which are correlated with SBS40b) and incidence of kidney cancer within each country. This correlation reflects approximately a tripling of average country-specific SBS40b mutation loads (a difference of ~1000 mutations) in parallel with the eightfold increase of country-specific ASR.

SBS40b mutation burdens also positively correlated with biomarkers of impaired kidney function, reminiscent of the nephrotoxic effects of Aristolochic acids in Balkan endemic nephropathy. It is possible that the increased SBS40b somatic mutation load itself engenders this reduction in renal function. However, studies of other normal tissues suggest that they are

generally tolerant of elevated mutation burdens, except for manifesting a higher incidence of neoplasia[33,34]. It is also possible that the agent underlying SBS40b is directly nephrotoxic, for example by engendering DNA damage and a response to it, and that the mutations it generates are immaterial to kidney function. It is also conceivable, however, that impaired renal function, potentially due to many different causes, results in a metabolic state which itself causes the elevated SBS40b mutation load. Whatever the mutational process underlying SBS40b, it is plausible that it contributes to the geographical variation in the age standardized rates of kidney cancer incidence rates. It is of public health interest to determine the cause of SBS40b and, hence, to consider whether the exposure can be mitigated, potentially with concomitant reduction in global ccRCC incidence rates.

Finally, it is notable that overall tumor mutation burden did not vary substantially between countries, with most variation being due to mutations linked to Aristolochic acid, and had only a weak association with overall kidney cancer incidence (**Extended Data Fig. 1 and 8)**. Along with an absence of any association between several known risk factors for ccRCC and mutation burden, in particular for obesity and hypertension, these results provide further evidence for a model of cancer development where mutations are essential but additional factors affect the expansion of a mutated clone and thus the chance of it progressing into cancer[35]. Further efforts at defining how lifestyle and environmental exposures contribute to cancer development will therefore require a greater understanding of both the causes of the mutations in cell clones in normal tissue, and the further promotion of such mutant clones by non-mutagenic processes.

REFERENCES

1. Brennan, P. & Davey-Smith, G. Identifying Novel Causes of Cancers to Enhance Cancer Prevention: New Strategies Are Needed. *JNCI: Journal of the National Cancer Institute* **114**, 353–360 (2022).

2. Hsieh, J. J. *et al.* Renal cell carcinoma. *Nat Rev Dis Primers* **3**, 17009 (2017).

3. Shearer, J. J. *et al.* Serum Concentrations of Per- and Polyfluoroalkyl Substances and Risk of Renal Cell Carcinoma. *J Natl Cancer Inst* **113**, 580–587 (2021).

4. Koh, G., Degasperi, A., Zou, X., Momen, S. & Nik-Zainal, S. Mutational signatures: emerging concepts, caveats and clinical applications. *Nat Rev Cancer* **21**, 619–637 (2021).

5. Alexandrov, L. B. *et al.* The repertoire of mutational signatures in human cancer. *Nature* **578**, 94–101 (2020).

6. Scelo, G. *et al.* Variation in genomic landscape of clear cell renal cell carcinoma across Europe. *Nat Commun* **5**, 5135 (2014).

7. Mitchell, T. J. *et al.* Timing the Landmark Events in the Evolution of Clear Cell Renal Cell Cancer: TRACERx Renal. *Cell* **173**, 611-623.e17 (2018).

8. Campbell, P. J. *et al.* Pan-cancer analysis of whole genomes. *Nature* **578**, 82–93 (2020).

9. Degasperi, A. *et al.* A practical framework and online tool for mutational signature analyses show intertissue variation and driver dependencies. *Nat Cancer* **1**, 249–263 (2020).

10. The Cancer Genome Atlas Research Network. Comprehensive molecular characterization of clear cell renal cell carcinoma. *Nature* **499**, 43–49 (2013).

11. Mutographs Cancer Grand Challenge. *https://cancergrandchallenges.org/teams*.

12. Sung, H. *et al.* Global Cancer Statistics 2020: GLOBOCAN Estimates of Incidence and Mortality Worldwide for 36 Cancers in 185 Countries. *CA Cancer J Clin* **71**, 209–249 (2021).

13. Nik-Zainal, S. *et al.* Mutational Processes Molding the Genomes of 21 Breast Cancers. *Cell* **149**, 979–993 (2012).

14. Alexandrov, L. B. *et al.* Signatures of mutational processes in human cancer. *Nature* **500**, 415–421 (2013).

15. Drost, J. *et al.* Use of CRISPR-modified human stem cell organoids to study the origin of mutational signatures in cancer. *Science (1979)* **358**, 234–238 (2017).

16. Hoang, M. L. *et al.* Mutational Signature of Aristolochic Acid Exposure as Revealed by Whole-Exome Sequencing. *Sci Transl Med* **5**, (2013).

17. Poon, S. L. *et al.* Genome-wide mutational signatures of aristolochic acid and its application as a screening tool. *Sci Transl Med* **5**, 197ra101 (2013).

18. Grollman, A. P. Aristolochic acid nephropathy: Harbinger of a global iatrogenic disease. *Environ Mol Mutagen* **54**, 1–7 (2013).

19. Turesky, R. J. *et al.* Aristolochic acid exposure in Romania and implications for renal cell carcinoma. *Br J Cancer* **114**, 76–80 (2016).

20. Wang, X.-M. *et al.* Integrative genomic study of Chinese clear cell renal cell carcinoma reveals features associated with thrombus. *Nat Commun* **11**, 739 (2020).

21. Huang, M. N. *et al.* Genome-scale mutational signatures of aflatoxin in cells, mice, and human tumors. *Genome Res* **27**, 1475–1486 (2017).

22. Dempsey, D. *et al.* Nicotine metabolite ratio as an index of cytochrome P450 2A6 metabolic activity. *Clin Pharmacol Ther* **76**, 64–72 (2004).

23. Velenosi, T. J. *et al.* Untargeted metabolomics reveals N, N, N-trimethyl-L-alanyl-L-proline betaine (TMAP) as a novel biomarker of kidney function. *Sci Rep* **9**, 6831 (2019).

24. Sato, Y. *et al.* Integrated molecular analysis of clear-cell renal cell carcinoma. *Nat Genet* **45**, 860–867 (2013).

25. Nik-Zainal, S. *et al.* The life history of 21 breast cancers. *Cell* **149**, 994–1007 (2012).

26. Dentro, S. C., Wedge, D. C. & van Loo, P. Principles of Reconstructing the Subclonal Architecture of Cancers. *Cold Spring Harb Perspect Med* **7**, (2017).

27. Nik-Zainal, S. *et al.* The genome as a record of environmental exposure. *Mutagenesis* gev073 (2015) doi:10.1093/mutage/gev073.

28. Kucab, J. E. *et al.* A Compendium of Mutational Signatures of Environmental Agents. *Cell* **177**, 821-836.e16 (2019).

29. Gabriel, A. A. G. *et al.* Genetic Analysis of Lung Cancer and the Germline Impact on Somatic Mutation Burden. *JNCI: Journal of the National Cancer Institute* **114**, 1159–1166 (2022).

30. Liu, Y., Gusev, A., Heng, Y. J., Alexandrov, L. B. & Kraft, P. Somatic mutational profiles and germline polygenic risk scores in human cancer. *Genome Med* **14**, 14 (2022).

31. Moody, S. *et al.* Mutational signatures in esophageal squamous cell carcinoma from eight countries with varying incidence. *Nat Genet* **53**, 1553–1563 (2021).

32. Abascal, F. *et al.* Somatic mutation landscapes at single-molecule resolution. *Nature* **593**, 405–410 (2021).

33. Martincorena, I. *et al.* High burden and pervasive positive selection of somatic mutations in normal human skin. *Science (1979)* **348**, 880–886 (2015).

34. Martincorena, I. *et al.* Somatic mutant clones colonize the human esophagus with age. *Science (1979)* **362**, 911–917 (2018).

35. Fowler, J. C. & Jones, P. H. Somatic Mutation: What Shapes the Mutational Landscape of Normal Epithelia? *Cancer Discov* **12**, 1642–1655 (2022).

FIGURE AND TABLE LEGENDS

Fig. 1: Eleven participating countries and estimated age-standardized incidence rates of clear cell renal cell carcinomas.

Incidence of clear cell renal cell carcinomas (ccRCC), men and women combined, age-standardized incidence rates (ASR) per 100,000, data from GLOBOCAN 2020. Markers indicate countries included in this study (number of participating ccRCC patients per country).

Table 1. Summary of clear cell renal cell carcinomas risk factors included in this study.

Fig. 2: Single base substitution signature operative in clear cell renal cell carcinomas. **(a)** TMB plot showing the frequency and mutations per Mb for each of the decomposed SBS signatures. **(b)** Average relative attribution for single base substitution (SBS) signatures across countries. Signatures contributing less than 5% on average are grouped in the 'Others' category, apart from SBS12 and AA-related signatures SBS22a and SBS22b. '<95% confidence' category accounts for the proportion of mutation burden which could not be assigned to any signature with confidence level of at least 95%. **(c)** Decomposed signatures, including reference COSMIC signatures as well as *de novo* signatures not decomposed into COSMIC reference signatures.

Fig. 3: Geospatial analysis of Aristolochic acid-related SBS signatures. Distribution of Romanian and Serbian cases with known residential history, along with the summed levels of SBS22a and SBS22b attributions (per-case and regional estimate), with respect to the Balkan endemic nephropathy (BEN) areas. White circles represented cases with no detected activity of SBS22a and SBS22b.

Fig. 4: Association of SBS40b signature attribution with incidence of kidney cancer. **(a)** Number of mutations attributed to signature SBS40b against age-standardized incidence rates (ASR) of kidney cancer in each of the eleven countries represented in the cohort. **(b)** Number of mutations attributed to signature SBS40b in four regions of Czech Republic against ASR of kidney cancer in each region. **(c)** Levels of attribution of SBS40b signature within Czech Republic, with bar plots showing the number of cases for each quartile of SBS40b attribution across Prague, Olomouc, Ceske Budejovice, and Brno regions.

Fig. 5: Driver mutation analysis in clear cell renal cell carcinomas. **(a)** Frequency of driver genes in the cohort. Only genes mutated in at least 10 cases are shown. **(b)** Frequency of driver genes across countries. **(c)** SBS-96 mutational spectra of all driver mutations in ccRCC for Aristolochic acid (AA)-exposed and unexposed cases. **(d)**

Percentage of T>A driver mutations in AA-exposed and unexposed cases. **(e)** SBS-96 mutational spectra of VHL mutations in ccRCC for AA-exposed and unexposed cases. **(f)** Percentage of T>A VHL mutations in AA-exposed and unexposed cases.

ONLINE METHODS

Recruitment of cases and informed consent

The International Agency for Research on Cancer (IARC/WHO) coordinated case recruitment through an international network of over 40 collaborators from the 11 participating countries (**Table1**; **Supplementary table 12**). The inclusion criteria for patients were >=18 years of age (ranging from 23 to 87, with a mean of 60 and a standard deviation of 12), confirmed diagnosis of primary ccRCC and no prior cancer treatment. Informed consent was obtained for all participants. Patients were excluded if they had any condition that could interfere with their ability to provide informed consent or if there were no means of obtaining adequate tissues or associated data as per the protocol requirements. Ethical approvals were first obtained from each Local Research Ethics Committee and Federal Ethics Committee when applicable, as well as from the IARC Ethics Committee.

Bio-samples, data collection, and expert pathology review

Dedicated standard operating procedures, following guidelines from the International Cancer Genome Consortium (ICGC), were designed by IARC/WHO to select appropriate case series with complete biological samples and exposure information as described previously[1] (**Supplementary Table 12**). In brief, for all case series included, anthropometric measures were taken, together with relevant information regarding medical and familial history. Comparable smoking and alcohol history was available from all centers. Detailed epidemiological information on residential history was collected in Czech Republic, Romania, and Serbia. Potential limitations of using retrospective clinical data collected using different protocols from different populations were addressed by a central data harmonization to ensure a comparable group of exposure variables (**Supplementary Table 12**). All patient related data as well as clinical, demographical, lifestyle, pathological and outcome data were pseudonymized locally through the use a dedicated alpha-numerical identifier system before being transferred to IARC/WHO central database.

Original diagnostic pathology departments provided diagnostic histological details of contributing cases through standard abstract forms. IARC/WHO centralized the entire pathology workflow and coordinated a centralized digital pathology examination of the frozen tumor tissues collected for the study as well as formalin-fixed, paraffin-embedded (FFPE) sections when available, via a web-based report approach and dedicated expert panel following standardized procedures as described previously[1]. A minimum of 50% viable tumor cells was required for eligibility to whole genome sequencing.

In summary, frozen tumor tissues were first examined to confirm the morphological type and the percentage of viable tumor cells. A random selection of tumor tissues was independently evaluated by a second pathologist. Enrichment of tumor component was performed by dissection of non-tumoral part, if necessary.

DNA extraction

Extraction of DNA from fresh frozen tumor and matched blood samples was centrally conducted at IARC/WHO except for Japan, which performed DNA extractions at the local center following a similarly standardized DNA extraction procedure. Of the cases which proceeded to the final analysis (*n*=962), germline DNA was extracted from either buffy-coat, whole blood, or from adjacent normal tissue (*viz.*, samples from Japan) using previously described protocols and methods[1].

Whole genome sequencing

In total, 1583 renal cell carcinoma cases were evaluated, with 1267 confirmed as ccRCC cases. 116 (9%) were excluded due to insufficient viable tumor cells (pathology level), or inadequate DNA (tumor or germline). DNA from 1151 cases was received at the Wellcome Sanger Institute for whole genome sequencing. Fluidigm SNP genotyping with a custom panel was performed to ensure that each pair of tumor and matched normal samples originated from the same individual. Whole genome sequencing (150bp paired end) was performed on the Illumina NovaSeq 6000 platform with target coverage of 40X for tumors and 20X for matched

normal tissues. All sequencing reads were aligned to the GRCh38 human reference genome using Burrows-Wheeler-MEM (v0.7.16a and v0.7.17). Post-sequencing QC metrics were applied for total coverage, evenness of coverage and contamination. Cases were excluded if coverage was below 30X for tumor or 15X for normal tissue. For evenness of coverage, the median over mean coverage (MoM) score was calculated. Tumors with MoM scores outside the range of values determined by previous studies to be appropriate for whole genome sequencing (0.92 – 1.09) were excluded. Conpair[2] (https://github.com/nygenome/Conpair) was used to detect contamination, cases were excluded if the result was greater than 3%[3]. A total of 962 cases passed all criteria and were included in subsequent analysis.

Somatic variant calling

Variant calling was performed using the standard Sanger bioinformatics analysis pipeline (https://github.com/cancerit). Copy number profiles were determined first using the algorithms ASCAT[4] and BATTENBERG[5], where tumor purity allowed. SNV were called with cgpCaVEMan[6], indels were called with cgpPINDEL[7], and structural rearrangements were called using BRASS. CaVEMan and BRASS were run using the copy number profile and purity values determined from ASCAT where possible (complete pipeline, n=857). Where tumor purity was insufficient to determine an accurate copy number profile (partial pipeline, n=105), CaVEMan and BRASS were run using copy number defaults and an estimate of purity obtained from ASCAT/BATTENBERG. For SNV additional filters (ASRD >= 140 and CLPM ==0) were applied to remove potential false positive calls. To further exclude the possibility of caller specific artefacts being included in the analysis, a second variant caller, Strelka2, was run for SNVs and indels[1,8]. Only variants called by both the Sanger variant calling pipeline and Strelka2 were included in subsequent analysis.

Validation of Japanese sequencing

The matched normal tissue sequenced was blood for all countries with the exception of Japan, where adjacent normal kidney was used. As Japan displayed an enrichment of SBS12,

583 matched blood was obtained from 28 of the 36 patients to confirm that the source of the
584 matched normal tissue was not influencing the result. In all cases, the mutational spectra of
585 Japanese ccRCC generated using either blood or adjacent normal kidney matched each other
586 with a cosine similarity of >0.99.
587
588 **Generation of mutational matrices**
589 Mutational matrices for single base substitutions (SBS), doublet base substitutions (DBS) and
590 small insertions and deletions (ID) were generated using SigProfilerMatrixGenerator
591 (https://github.com/AlexandrovLab/SigProfilerMatrixGenerator) with default options (v1.2.12)[9].
592
593 **Mutational signature analysis**
594 Mutational signatures were extracted using two algorithms, SigProfilerExtractor
595 (https://github.com/AlexandrovLab/SigProfilerExtractor), based on nonnegative matrix
596 factorization, and mSigHdp[10] (https://github.com/steverozen/mSigHdp), based on the
597 Bayesian hierarchical Dirichlet process. For SigProfilerExtractor, *de novo* mutational
598 signatures were extracted from each mutational matrix using SigProfilerExtractor with
599 nndsvd_min initialization (NMF_init="nndsvd_min") and default parameters (v1.1.9)[11]. Briefly,
600 SigProfilerExtractor deciphers mutational signatures by first performing Poison resampling of
601 the original matrix with additional renormalization (based on a generalized mixture model
602 approach) of hypermutators to reduce their effect on the overall factorization[11]. Nonnegative
603 matrix factorization (NMF) was performed using initialization with nonnegative singular value
604 decomposition and by applying the multiplicative update algorithm using the Kullback–Leibler
605 divergence as an objective function[11]. NMF was applied with factorizations between k=1 and
606 k=20 signatures; each factorization was repeated 500 times[11]. *De novo* single base
607 substitution mutational signatures were extracted with SigProfilerExtractor for both SBS-288
608 and SBS-1536 contexts[9]. The results were largely concordant with the SBS-1536 *de novo*
609 signatures allowing additional separation of mutational processes, therefore the SBS-1536 *de*
610 *novo* signatures were taken forward for further analysis (**Supplementary Table 2**). Mutational

signatures for DBS and ID were extracted in DBS-78 and ID-83 contexts respectively (**Supplementary Tables 3 & 4**). Where possible, SigProfilerExtractor matched each *de novo* extracted mutational signature to a set of previously identified COSMIC signatures[12], for SBS-1536 signatures this requires collapsing the 1536 classification into the standard 96 substitution type classification with six mutation classes having single 3' and 5' sequence contexts (Supplementary Table **5**). This step makes it possible to distinguish between *de novo* signatures which can be explained by a combination of the known catalog of mutational process (which have not been completely separated during the extraction), and those which have not been previously identified. mSigHdp extraction of SBS-96 and ID-83 signatures was performed using the suggested parameters and using the country of origin to construct the hierarchy. SigProfilerExtractor's decomposition module was subsequently used to match mSigHdp *de novo* signatures to previously identified COSMIC signatures[12]. Further details on the comparison of results between SigProfilerExtractor and mSigHdp and decomposition of *de novo* signatures into COSMIC reference signatures can be found in the supplementary note.

Attribution of activities of mutational signatures

The *de novo* (SigProfiler) and COSMIC signature (SigProfiler and mSigHdp) activities were attributed for each sample using the MSA signature attribution tool (v2.0, https://gitlab.com/s.senkin/MSA)[13]. For COSMIC attributions, only COSMIC reference signatures, which were identified in the decomposition of *de novo* signatures, where included in the panel for attribution, in addition to *de novo* signatures which could not be decomposed into COSMIC reference. At its core, the tool utilizes the nonnegative least squares (NNLS) approach minimizing the L2 distance between the input sample and the one reconstructed using available signatures. To limit false positive attributions, automated optimization procedure was applied by repeated removal of all signatures that do not increase the L2 similarity of a sample by >0.008 for SBS, >0.014 for DBS, and >0.03 for ID mutation types, as suggested by simulations. These optimal penalties were derived using an optional parameter (params.no_CI_for_penalties = false) utilizing a conservative approach in calculation of

639 penalties. Finally, a parametric bootstrap approach was applied to extract 95% confidence
640 intervals for each attributed mutational signature activity.
641
642 **Driver mutations**
643 A dNdS approach was used to identify genes under positive selection in ccRCC[14]. The analysis
644 was preformed both for the whole genome (q-value<0.01), and with restricted hypothesis
645 testing (RHT) for a panel of 369 known cancer genes[14]. Variants in any gene identified as
646 under positive selection in global dNdS or in the 369-cancer gene panel were assessed as
647 potential drivers[14]. Candidate driver mutations were annotated with the mode of action using
648 the Cancer Gene Census (https://cancer.sanger.ac.uk/census) and the Cancer Genome
649 Interpreter tool (https://www.cancergenomeinterpreter.org). Missense mutations were
650 assessed using the MutationMapper tool (http://www.cbioportal.org/mutation_mapper).
651 Variants were considered likely drivers if they met any of the following criteria: *(i)* Truncating
652 mutations in genes annotated as tumor suppressors; *(ii)* mutations annotated as likely or
653 known oncogenic in MutationMapper; (iii) truncating variants in genes with selection (q-
654 value<0.05) for truncating mutations assumed to be tumor suppressors and thus likely drivers;
655 *(iv)* missense variants in all genes under positive selection and with dN/dS ratios for missense
656 mutations above 5 (assuming 4 of every 5 missense mutations are drivers) labelled as likely
657 drivers; or *(v)* in-frame indels in genes under significant positive selection for in-frame indels.
658
659 **Evolutionary analysis**
660 Subclonal architecture reconstruction was performed using the DPClust R package v2.2.8[5,15],
661 after obtaining cancer cell fraction (CCF) estimates by dpclust3p v1.0.8
662 (https://github.com/Wedge-lab/dpclust3p) based on the variant allele frequency provided by
663 the somatic variant callers and the copy number profiles determined by the BATTENBERG
664 algorithm. Only tumors with at least 40% purity according to BATTENBERG were considered
665 for further evolutionary analysis. For each tumor with at least one subclone, the respective
666 somatic mutations were split into clonal and subclonal mutations using the most probable

667 cluster assignment for each mutation as per the DPClust output. Mutations not assigned to a
668 cluster by DPClust were removed from further analysis. Clusters centered at a CCF>1.5 and
669 ones where chromosome X contributed the highest number of mutations were deemed
670 artifactual, and the respective mutations were removed. Samples with a total number of clonal
671 or subclonal mutations below 256 were also removed. Additionally, samples with poor
672 separation between the clonal and subclonal distributions (*e.g.*, subclone centered at a
673 CCF>0.80) were removed. Finally, only samples that had both a clone and at least one
674 subclone post-filtering were retained for further analysis. This yielded a total of 223 samples,
675 each with clonal and subclonal mutations. SigProfilerAssignment (v0.0.13)
676 (https://github.com/AlexandrovLab/SigProfilerAssignment) was used to identify the activity of
677 each mutational signature in each clone/subclone, and these activities were then normalized
678 by the total number of mutations belonging to the clone/subclone (*i.e.*, clonal mutations were
679 not included in the subclone). A two-sided Wilcoxon Signed-Rank Test[16] was used to assess
680 the differences in the relative activity of each mutational signature between the clones and
681 their respective subclones. P-values were corrected using the Benjamini-Hochberg
682 procedure[17] and reported as q-values in the manuscript.
683
684 **Regressions**
685 Signature attributions were dichotomized into presence and absence using confidence
686 intervals, with presence defined as both lower and upper limits being positive, and absence as
687 the lower limit being zero. If a signature was present in at least 75% of cases (SBS1, SBS40a,
688 SBS40b, ID1, and ID5), it was dichotomized into above and below the median of attributed
689 mutation counts. The binary attributions served as dependent variables in logistic regressions,
690 and relevant risk factors were used as factorized independent variables. To adjust for
691 confounding factors, sex, age of diagnosis, country, and tobacco status were added as
692 covariates in regressions. The Bonferroni method was used to test for significant p-values (*i.e.,*
693 a total of 224 comparisons for regressions with signatures, and a total of 24 comparisons for
694 regressions with mutation burden). P-values reported are raw (not corrected). Regressions

with incidence of renal cancer were performed as linear regressions with mutation burdens or signature attributions with confidence intervals not consistent with zero as a dependent variable, and age-standardized rates (ASR) of renal cancer obtained from Global Cancer Observatory (GLOBOCAN)[18], sex and age of diagnosis as independent variables. ASR of renal cancer for regions of Czech Republic were obtained from SVOD web portal[19].

Polygenic risk score (PRS) analysis of lifestyle risk factors

In this analysis, we used the genome-wide association studies (GWAS) summary statistics estimated in European populations for well-established risk factors for ccRCC. For tobacco smoking status, we used results from the GSCAN consortium meta-analysis of smoking initiation (ever vs never status)[20]. For body mass index (BMI), the results of UK biobank (UKBB) meta-analysis of continuous BMI were used[21]. GWAS summary statistics related to hypertension, namely systolic blood pressure and diastolic blood pressure, as well as the ones related to diabetes[22], such as fasting glucose and fasting insulin were also obtained using UKBB studies[23].

Since all the GWAS summary statistics used in the current work were based on European populations, we used ADMIXTURE tool (v1.3.0)[24] and principal component analysis (PCA) to infer the unsupervised cluster of individuals with European genetic background within ccRCC cases. Hapmap SNPs (n=1,176,821 variants) were extracted from the ccRCC whole-genome sequence genotype data. After basic quality control using PLINK (v1.9b, www.cog-genomics.org/plink/1.9/), 333 variants were removed due to missing genotype rate > 5%, 1,236 variants failed Hardy-Weinberg equilibrium test (p-values<10^{-8}), and 18,702 variants had MAF<1% in our cohort. Additionally, 3 ambiguous variants and 21,358 variants within regions of long-range, high linkage disequilibrium (LD) in the human genome (hg38) were excluded. After pruning for linkage disequilibrium, 143,727 variants remained in ccRCC genotype data. The 1000 genome reference population genotype data (phase 3) for Europeans (N=489), Africans (YRI, N=108) and East Asians (N=103 from China and 104 from Japan)

(https://www.internationalgenome.org/data/) were filtered and merged with ccRCC genotype data based on the pruned set of variants present in both datasets. ADMIXTURE was run on the merged genotype data with *k*=3, which would correspond to the three ancestral continental population groups that likely reflect the participants of our study. The ccRCC cases with European genetic fraction greater than 80% by the ADMIXTURE analysis were selected for the polygenic risk scores (PRS) analyses. To complement the ADMIXTURE analysis, PCA was run on the same samples.

The initial genotype data based on whole-genome sequence from 849 ccRCC cases with European genetic background consisted of biallelic SNPs with MAF >0.01% (to exclude ultra-rare variants; N ~ 30 million variants). After basic quality control, variants with missing genotype rate of greater than 5% (N=7,519,196 variants) with strong deviation from Hardy-Weinberg equilibrium (p-values<10^{-8}, N=220,862) were excluded. For each GWAS trait, we restricted our analyses to the biallelic SNPs with minor allele frequency (MAF) greater than 1% in the 1000 genomes reference for European populations. For the selection of the independent genome-wide significant hits (p-values<5×10^{-8}) of each GWAS summary statistic used to generate the PRS, SNPs were clumped (r^2=0.1 within a LD window of 10 MB) using PLINK (v1.9b, www.cog-genomics.org/plink/1.9/) based on the 1000 genomes European reference population genotype data (N=489; ~ 10 million variants). Where a selected GWAS hit was not found in ccRCC genotype data, we extracted proxies (r^2>0.8 in 1000 genomes) also present in ccRCC dataset where possible (**Supplementary Table 11**). The variance of each genetic trait explained by the genetic variants were calculated as previously suggested[25]. PRS was subsequently calculated as the sum of the individual's beta-weighted genotypes using PRSice-2 software[26]. Associations were estimated per standard deviation increase in the PRS, which was normalized to have a mean of zero across ccRCC cases of European genetic ancestry.

Untargeted metabolomics association with signatures

Of the 962 subjects from the main analysis, 901 subjects were included in this sub-study – all Japanese samples (*n*=36) as well as few cases from Czech Republic (*n*=13), Romania (*n*=5) and Russia (*n*=3) were not included due to lack of available plasma samples. Samples were randomized and analyzed as two independent analytical batches. Analysis was performed with a UHPLC-QTOF-MS system that consisted of a 1,290 Binary LC and a 6,550 QTOF mass spectrometer equipped with Jet Stream electrospray ionization source (Agilent Technologies), using previously described methods[27]. Pre-processing was performed using Profinder 10.0.2.162 and Mass Profiler Professional B.14.9.1 software (Agilent Technologies). A "Batch recursive feature extraction (small molecules)" process was employed for samples and blanks to find $[M+H]^+$ ions. The two batches were processes separately and the resulting features were aligned in Mass Profiler Professional. Chromatographic peak areas were used as a measurement of intensity.

A total of 2,392 features were detectable in at least one of the 901 samples. Features present in only one of the two batches were filtered out. Recursive filtering elimination was applied to decrease redundancy from highly correlated variables (r≥0.85, Pearson's r calculated before any transformation/imputation) by selecting the features with least missing data within clusters of features. A total of 944 features were included in the statistical analysis. Features were pre-processed: missing values were replaced with 1/5 of the minimal value of the feature before applying mean centering and Pareto scaling. Each feature was regressed against both *de novo* and COSMIC signatures, adjusting for sex and age of diagnosis, as well as body mass index (BMI) and technical factors (batch, acquisition order) that could impact chromatographic peak area. Models for SBS22a and SBS22b were restricted to Romanian and Serbian samples to find potential pathways of Aristolochic acid exposure in the Balkan region. Logistic models were used for zero-inflated signatures (≥30% zeros) while quasi-Poisson regressions were used for the least zero-inflated signatures (SBS1, SBS40a, and SBS40b). To derive specific false detection rates, random variables were created from permutations of the initial features

and regressed against signatures in the same fashion as true features. Maximum p-value thresholds from regressions with random features were compared to adjusted p-value thresholds according to Bonferroni's procedure. The more conservative approach was used in selecting features of interest. Random forest models were also used as cross-checking multivariate models to assess the relative importance of each feature in explaining the signature attribution. As with univariate models, regression models were used for the least zero-inflated signatures (<30% of zeros) while classification models were used for all other signatures, with restriction to Romanian and Serbian samples for SBS22a and SBS22b. Importance was estimated from the total decrease in node impurities from splitting on the variable, averaged over all trees. Node impurity was measured by the Gini index for classification, and by residual sum of squares for regression. The significance of importance metrics for Random Forest models were estimated by permuting the response variable (https://github.com/EricArcher/rfPermute).

Features considered for identification, along with their highly correlated counterparts, were searched in Human Metabolome Database (HMDB), LipidMaps, Metlin, and Kegg. Compound identity was confirmed by comparison of retention times and MS/MS fragmentation against chemical standards when available, or otherwise against reference MS/MS spectra. Since the feature 240.1468@0.8929933 was strongly correlated with several features identified as TMAP (Supplementary Table 13), the integration of these features was inspected and corrected manually, and regressed against SBS40b using the same model applied to features selected for analysis. Creatinine was identified among the features by matching its retention time and MS/MS spectra against a reference standard and also regressed against SBS40b in the same fashion as other metabolites. Estimation of correlation between metabolic features was done using linear regression adjusting for batch and acquisition order.

807 **Targeted metabolomics analyses**

808 Circulating levels of PFAS (Per- and Polyfluorinated Substances) and cystatin C compounds
809 were investigated using targeted mass spectrometry-based methods as described
810 previously[28,29].

811

812 Out of the 962 subjects from the main analysis, plasma samples from 909 subjects (from all
813 countries except Japan) were randomized and sent frozen in dry ice to each respective
814 laboratory for analyses. Measurement of cystatin C from 906 subjects included its native form
815 and isoforms (3Pro-OH cystatin C, cystatin C-desS, 3Pro-OH cystatin C-desS and cystatin C-
816 desSSP) that were modeled individually and for the total concentration of cystatin C isoforms.
817 Measurements of PFAS compounds included PFOA (Perfluorooctanoic Acid; total, branch,
818 linear), PFOS (Perfluorooctanoic Acid; total, branch, linear), PFHxS (Perfluorohexane
819 sulfonate), PFNA (Perfluorononanoic acid), PFDA (Perfluorodecanoic acid), MePFOSAA (n-
820 methylperfluoro-1 octanesulfonamido acetic acid), EtPFOSAA (2-(N-Ethyl-perfluorooctane.
821 sulfonamido) acetic acid).

822

823 Multivariable quasi-Poisson (for the least sparse signatures SBS1, SBS40a and SBS40b) and
824 logistic regression were used to estimate the association between plasma concentrations of
825 the aforementioned substances and mutational signatures. All compounds were modeled
826 continuously (log2-transformed) and categorically, with adjustments made by sex, age, date
827 of recruitment, country, BMI, tobacco and alcohol status in the case of PFAS molecules and
828 by sex, age and BMI, in the case of cystatin C.

829

830 **Geospatial analyses**

831 Geospatial analyses were performed to estimate the regional effect for signature attribution,
832 particularly for signatures thought to be from exogenous exposure (SBS40b – unknown – and
833 SBS22a/SB22b - Aristolochic acid). Residential history information was available for a large
834 proportion of cases from the countries of interest: Czech Republic for SBS40b and

Romania/Serbia for SBS22a/SBS22b. The 259 cases from Czech Republic within this study were recruited from 4 separate regions including Prague, České Budějovice (in Southern Bohemia), as well as Brno and Olomouc in the east of the country. Each individual residence was geocoded to its administrative region. All locations outside the country of recruitment were labeled as "Abroad". A multi-membership mixed model was used to account for the full list of regions in which each subject resided, as well as the proportion of life spent in that region before diagnosis. As dependent variable, signatures were inverse-normal transformed. Models were adjusted for sex and age of diagnosis (fixed effects). The regional effect was treated as random effect.

Data availability

Whole genome sequencing data and patient metadata are deposited in the European Genome-phenome Archive (EGA) associated with study EGAS00001003542. All other data is provided in the accompanying Supplementary Tables.

Code availability

All algorithms used for data analysis are publicly available with repositories noted within the respective method sections and in the accompanying reporting summary. Code used for regression analysis and figures is available at:
https://gitlab.com/Mutographs/Mutographs_RCC.

Methods references

1. Moody, S. *et al.* Mutational signatures in esophageal squamous cell carcinoma from eight countries with varying incidence. *Nat Genet* **53**, 1553–1563 (2021).
2. Whalley, J. P. *et al.* Framework for quality assessment of whole genome cancer sequences. *Nat Commun* **11**, 5040 (2020).

3. Bergmann, E. A., Chen, B.-J., Arora, K., Vacic, V. & Zody, M. C. Conpair: concordance and contamination estimator for matched tumor–normal pairs. *Bioinformatics* **32**, 3196–3198 (2016).

4. Van Loo, P. *et al.* Allele-specific copy number analysis of tumors. *Proceedings of the National Academy of Sciences* **107**, 16910–16915 (2010).

5. Nik-Zainal, S. *et al.* The life history of 21 breast cancers. *Cell* **149**, 994–1007 (2012).

6. Jones, D. *et al.* cgpCaVEManWrapper: Simple Execution of CaVEMan in Order to Detect Somatic Single Nucleotide Variants in NGS Data. *Curr Protoc Bioinformatics* **56**, (2016).

7. Raine, K. M. *et al.* cgpPindel: Identifying Somatically Acquired Insertion and Deletion Events from Paired End Sequencing. *Curr Protoc Bioinformatics* **52**, (2015).

8. Kim, S. *et al.* Strelka2: fast and accurate calling of germline and somatic variants. *Nat Methods* **15**, 591–594 (2018).

9. Bergstrom, E. N. *et al.* SigProfilerMatrixGenerator: a tool for visualizing and exploring patterns of small mutational events. *BMC Genomics* **20**, 685 (2019).

10. Liu, M., Wu, Y., Jiang, N., Boot, A. & Rozen, S. G. mSigHdp: hierarchical Dirichlet process mixture modeling for mutational signature discovery. *bioRxiv* 2022.01.31.478587 (2022) doi:10.1101/2022.01.31.478587.

11. Islam, S. M. A. *et al.* Uncovering novel mutational signatures by de novo extraction with SigProfilerExtractor. *Cell genomics* **2**, None (2022).

12. Alexandrov, L. B. *et al.* The repertoire of mutational signatures in human cancer. *Nature* **578**, 94–101 (2020).

13. Senkin, S. MSA: reproducible mutational signature attribution with confidence based on simulations. *BMC Bioinformatics* **22**, 540 (2021).

14. Martincorena, I. *et al.* Universal Patterns of Selection in Cancer and Somatic Tissues. *Cell* **171**, 1029-1041.e21 (2017).

15. Dentro, S. C., Wedge, D. C. & van Loo, P. Principles of Reconstructing the Subclonal Architecture of Cancers. *Cold Spring Harb Perspect Med* **7**, (2017).

16. Wilcoxon, F. Individual Comparisons by Ranking Methods. *Biometrics Bulletin* **1**, 80 (1945).

17. Benjamini, Y. & Hochberg, Y. Controlling the False Discovery Rate: A Practical and Powerful Approach to Multiple Testing. *Journal of the Royal Statistical Society: Series B (Methodological)* **57**, 289–300 (1995).

18. Sung, H. *et al.* Global Cancer Statistics 2020: GLOBOCAN Estimates of Incidence and Mortality Worldwide for 36 Cancers in 185 Countries. *CA Cancer J Clin* **71**, 209–249 (2021).

19. Dušek, L. *et al.* Epidemiology of Malignant Tumours in the Czech Republic [online]. Masaryk University, Czech Republic, [2005]. *http://www.svod.cz/. Version 7.0 [2007], ISSN 1802 – 8861*.

20. Liu, M. *et al.* Association studies of up to 1.2 million individuals yield new insights into the genetic etiology of tobacco and alcohol use. *Nat Genet* **51**, 237–244 (2019).

21. Yengo, L. *et al.* Meta-analysis of genome-wide association studies for height and body mass index in ~700000 individuals of European ancestry. *Hum Mol Genet* **27**, 3641–3649 (2018).

22. Lagou, V. *et al.* Sex-dimorphic genetic effects and novel loci for fasting glucose and insulin variability. *Nat Commun* **12**, 24 (2021).

23. Bycroft, C. *et al.* The UK Biobank resource with deep phenotyping and genomic data. *Nature* **562**, 203–209 (2018).

24. Alexander, D. H., Novembre, J. & Lange, K. Fast model-based estimation of ancestry in unrelated individuals. *Genome Res* **19**, 1655–1664 (2009).

25. Shim, H. *et al.* A Multivariate Genome-Wide Association Analysis of 10 LDL Subfractions, and Their Response to Statin Treatment, in 1868 Caucasians. *PLoS One* **10**, e0120758 (2015).

26. Choi, S. W. & O'Reilly, P. F. PRSice-2: Polygenic Risk Score software for biobank-scale data. *Gigascience* **8**, (2019).

27. Loftfield, E. *et al.* Novel Biomarkers of Habitual Alcohol Intake and Associations With Risk of Pancreatic and Liver Cancers and Liver Disease Mortality. *JNCI: Journal of the National Cancer Institute* **113**, 1542–1550 (2021).

28. Shearer, J. J. *et al.* Serum Concentrations of Per- and Polyfluoroalkyl Substances and Risk of Renal Cell Carcinoma. *J Natl Cancer Inst* **113**, 580–587 (2021).

29. Gao, J., Meyer, K., Borucki, K. & Ueland, P. M. Multiplex Immuno-MALDI-TOF MS for Targeted Quantification of Protein Biomarkers and Their Proteoforms Related to Inflammation and Renal Dysfunction. *Anal Chem* **90**, 3366–3373 (2018).

Acknowledgements

The authors would like to thank Laura O'Neill, Kirsty Roberts, Katie Smith, Maisie Farenden, Siobhan Austin-Guest and the staff of DNA Pipelines at the Wellcome Sanger Institute for their contribution. We are grateful for the support provided by Maja Milosevic, Christophe Lallemand, Helene Renard, Aude Bardot, Andreea Spanu and Nivonirina Robinot as well as IARC General Services, including the Laboratory Services and Biobank team led by Zisis Kozlakidis, the Section of Support to Research overseen by Tamas Landesz and the Evidence Synthesis and Classification Section led by Ian Cree, under IARC regular budget funding. The authors would like to thank Gislaine Bergo, Riley Cox and Juliana Oliveira for help with data/sample preparation and processing. The authors would also like to acknowledge the contributions of the Leeds Biobanking and Sample Processing Lab, the Leeds Multidisciplinary RTB and the Leeds NIHR BioRTB for provision of samples. The authors would like to thank Peter Campbell, Inigo Martincorena, Tim Butler, Daniela Mariosa, Laura Torrens Fontanals, Wellington Oliveira Dos Santos, Hana Zahed, Marc Gunter, Maggie Blanks and Mimi McCord for useful discussions. The authors would also like to thank all the patients and their families involved in this study.

Funding

This work was delivered as part of the Mutographs team supported by the Cancer Grand Challenges partnership funded by Cancer Research UK (C98/A24032). This work was supported by the Wellcome Trust grants 206194 and 220540/Z/20/A. The work was also partly funded by Barretos Cancer Hospital, the Public Ministry of Labor of Campinas (Research, Prevention, and Education of Occupational Cancer, 2015 to R.M.R.), and by Hospital de Clínicas de Porto Alegre (180330 to P.A.-P., M.B., B.S.N.). The work was also partly supported by the Practical Research Project for Innovative Cancer Control from the Japan Agency for Medical Research and Development (AMED) (JP20ck0106547h0001 to T.S.), and by the National Cancer Center Japan Research and Development Fund (2020-A-7 to A.F.). The work was also partly funded by the 1st and 2nd Faculties of Medicine, Charles University, Prague (CAGEKID to I.H.; Occupation, Environment and Kidney Cancer in Central and Eastern Europe to A.H.). The work was also partly supported by the Ministry of Health of the Czech Republic (MH CZ – DRO (MMCI, 00209805) to L.F. and M.N.). Measurement of PFAS compounds was funded by Division of Cancer Epidemiology and Genetics of the National Cancer Institute (USA). Measurement of cystatin C was funded by Cancer Research UK (C18281/A29019).

Contributions

The study was conceived, designed and supervised by M.R.S., P.B. and L.B.A. Analysis of data was performed by S.Senkin, S.Moody, M.D.-G., T.C., A.F.-I., J.W., S.F., M.K., R.V., A.P.L., E.N.B., A.K., B.O., S.C., E.T., J.A., K.S.-B., R.C.C.P., V.G., D.J., J.W.T. and J.M. Pathology review was carried out by B.A.-A., S.F. and M.A. Sample manipulation was carried out by C.L., C.C. and P.C. Patient and sample recruitment was led or facilitated by S.Sangkhathat, W.A., B.S., S.J., R.S., D.M., V.Jinga, S.R., S.Milosavljevic, M.M., S.Savic, J.M.S.B, M.A., L.P., P.A.-P., M.B., B.S.N., S.M.B., M.P.C., S.C.Z., R.M.R., E.F., N.S.M., R.S.F., R.B., N.V., D.Z., A.M., O.S., V.M., L.F., M.N., I.H., A.H., V.Janout, S.C. and C.L., M.P. P.K.-R., S.C., M.P., P.M.U. and M.J. contributed to data generation. Patient and sample

recruitment for Japanese cases was led by T.S. and A.F. Scientific project management was carried out by L.H., E.C., G.S., A.C.D.C., A.F.-I. and S.P. S.Moody and S.Senkin jointly contributed and were responsible for overall scientific coordination. The manuscript was written by S.Senkin, S.Moody, M.R.S. and P.B. with contributions from all other authors.

Competing interests

LBA is a compensated consultant and has equity interest in io9, LLC and Genome Insight. His spouse is an employee of Biotheranostics, Inc. LBA is also an inventor of a US Patent 10,776,718 for source identification by non-negative matrix factorization. ENB and LBA declare U.S. provisional applications with serial numbers: 63/289,601; 63/269,033; and 63/483,237. LBA also declares U.S. provisional applications with serial numbers: 63/366,392; 63/367,846; 63/412,835; and 63/492,348. VM received honoraria from Ipsen, Bayer, AstraZeneca, Janssen, Astellas Pharm and MSD, and provided expert testimony to BMS, Bayer, MSD and Janssen. No other authors declare any competing interests.

Disclaimer

Where authors are identified as personnel of the International Agency for Research on Cancer / World Health Organization, the authors alone are responsible for the views expressed in this article and they do not necessarily represent the decisions, policy or views of the International Agency for Research on Cancer / World Health Organization.

Corresponding author

Correspondence to Paul Brennan.

EXTENDED DATA FIGURE AND TABLE LEGENDS

Extended Data Fig. 1: Mutation burdens in clear cell renal cell carcinomas across countries.

Mutation burdens for single base substitutions (SBS) **(a)**, doublet base substitutions (DBS) **(b)** and small insertions and deletions (ID) **(c)** show significant differences between countries using the Kruskal-Wallis (two-sided) test (n=961 biologically independent samples). Four SBS hypermutators and four ID hypermutators above mutation burden of 30000 and 3000, respectively, were removed for clarity. Box and whiskers plots are in the style of Tukey. The line within the box is plotted at the median while the upper and lower ends are indicated 25th and 75th percentiles. Whiskers show 1.5*IQR (interquartile range) and values outside it are shown as individual data points.

Extended Data Fig. 2: Principal component analysis of relative mutation counts. PCA performed on relative mutation counts of all ccRCC tumors incorporating the six mutation classes (C>A, C>G, C>T, T>A, T>C, T>G). Principal component 1 (PC1) clearly separates the cluster of mostly Romanian cases that are enriched with AA signatures, often at high mutation burdens. Principal component 3 (PC3) identifies a cluster of mostly Japanese cases, enriched with signature SBS12.

Extended Data Fig. 3: Doublet-base substitution signatures operative in clear cell renal cell carcinomas.
(a) Tumour mutation burden (TMB) plot showing the frequency and mutations per Mb for each of the decomposed DBS signatures. **(b)** Average relative attribution for doublet-base substitution (DBS) signatures across countries. Signatures contributing less than 5% on average are grouped in the 'Other' category, apart from signature DBS_D. Category named '<95% confidence' accounts for the proportion of mutation burden which could not be assigned to any signature with confidence level of at least 95%. **(c)** Decomposed DBS signatures, including reference COSMIC signatures as well as *de novo* signatures not decomposed into COSMIC reference signatures.

Extended Data Fig. 4: Small insertions and deletion signatures operative in clear cell renal cell carcinomas.

(a) Tumour mutation burden (TMB) plot showing the frequency and mutations per Mb for each of the decomposed ID signatures. **(b)** Average relative attribution for small insertion and deletion (ID) signatures across countries. Signatures contributing less than 5% on average are grouped in the 'Others' category, apart from signature ID_C. Category named '<95% confidence' accounts for the proportion of mutation burden which could not be assigned to any signature with confidence level of at least 95%. **(c)** Decomposed ID signatures, including reference COSMIC signatures as well as *de novo* signatures not decomposed into COSMIC reference signatures.

Extended Data Fig. 5: Correlation amongst signatures SBS22a, SBS22b, DBS_D, ID_C.

Extended Data Table 1: Presence of signatures SBS22a, SBS22b, DBS_D, ID_C across countries.

Extended Data Fig. 6: Single base substitution signatures showing significant differences in attributed mutation burden between countries.

Signatures SBS40a **(a)** and SBS40b **(b)** were more prevalent in high-incidence regions of Czech Republic and Lithuania. Signatures SBS22a **(c)** and SBS22b **(d)** were enriched in Romania and Serbia. SBS1 **(e)**, SBS5 **(f)** and SBS4 **(g)** showed moderate differences across countries. Signature SBS12 **(h)** is highly prevalent in Japan. Five SBS1 hypermutators above mutation burden of 1000 were removed for clarity. Box and whiskers plots are in the style of Tukey. The line within the box is plotted at the median while the upper and lower ends are indicated 25th and 75th percentiles. Whiskers show 1.5*IQR (interquartile range) and values outside it are shown as individual data points.

Extended Data Fig. 7: Association of mutational signatures with incidence of renal cancer.

Number of mutations attributed to signatures **(a)** SBS40a, **(b)** ID5 and **(c)** ID8 against age-standardized incidence rate (ASR) of kidney cancer in each of the eleven countries represented in the cohort. The p-values shown are for ASR variable in linear regressions across all cases, adjusted for sex and age of diagnosis.

Extended Data Fig. 8: Association of mutation burden with incidence of renal cancer.

Association of age-standardized rates (ASR) of kidney cancer incidence with SBS (**a)**, DBS (**b)** and ID (**c)** mutation burdens across countries. Romania (ASR≈7.7) and Serbia (ASR≈7.4) were removed due to the region-specific exposure to Aristolochic acid, with AA-related signatures accounting for a large proportion of mutation burden in these countries. The p-values shown are for ASR variable in linear regressions across all cases, adjusted for sex and age of diagnosis.

Extended Data Fig. 9: Evolutionary analysis of mutational signatures in ccRCC.

Comparison of mutational signatures between clonal and subclonal mutations. Lines show the change in relative activity between the clonal mutations (main) and subclonal mutations (sub) within a sample. Blue and red lines represent an activity change of more than 6% (blue indicates higher in the clonal mutations; red indicates higher in the subclonal mutations). Bar plots show the distribution of activities in samples where the signature was present in the clonal and/or subclonal mutations; this number is represented in the title of each plot as X/223 for each signature. Black bars indicate one standard deviation away from the mean. Significance was assessed using a two-sided Wilcoxon signed-rank test, and q-values were generated using the Benjamini-Hochberg Procedure.

Fig.1

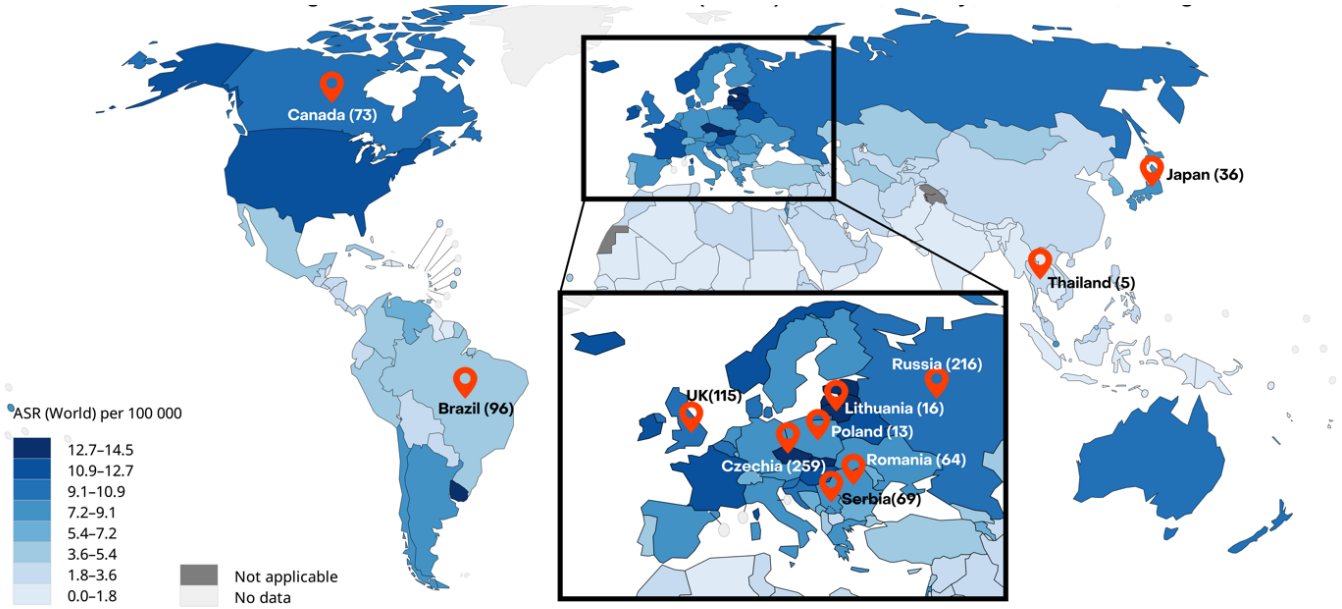

Data source: GLOBOCAN 2020
Map production: IARC
(http://gco.iarc.fr/today)
World Health Organization

Table 1

Country (ASR/100,000)		Brazil (4.5)	Canada (10.4)	Czechia (14.4)	Japan (7.6)	Lithuania (14.5)	Poland (8.1)	Romania (7.7)	Russia (10.3)	Serbia (7.4)	Thailand (1.8)	UK (10.3)	Total (4.6)
Number of cases		96	73	259	36	16	13	64	216	69	5	115	962
Sex	Female	44	22	93	8	9	5	25	98	30	4	42	380
	Male	52	51	166	28	7	8	39	118	39	1	73	582
	0-45	15	6	27	3	1	2	6	43	16	0	6	125
	45-55	20	17	51	5	0	6	10	44	11	0	22	186
Age at diagnosis	55-65	30	17	77	8	9	1	20	91	27	2	41	323
(years)	65-75	24	27	72	13	4	4	20	32	9	2	31	238
	75+	7	6	32	7	2	0	8	6	6	1	15	90
	1999-2005			93			13	14	18				138
Year of	2005-2010			111				19	70	1		31	232
recruitment	2010-2015		9	55	28			31	116	68		41	348
	2015-2020	96	64		8	16			12		5	43	244
	I	28	3	123	24	6	0	33	94	32		53	396
	II	2	0	42	1	0	6	12	24	4		8	99
Stage	III	16	23	46	6	5	5	18	65	26		38	248
	IV	7	10	38	5	2	2	1	33	7		16	121
	Missing	43	37	10		3					5		98
	<20	3	2	5	2	0	2	2	9	8	0	6	39
	20-25	21	10	100	25	2	3	17	84	28	3	23	316
Body mass index	25-30	35	24	85	7	6	6	30	40	20	1	45	299
	>30	37	37	69	2	8	2	14	83	13	1	41	307
	Missing							1					1
	No	45	28	129	16	5	9	39	125	28	2	58	484
Hypertension	Yes	51	44	130	20	10	4	24	91	41	3	56	474
	Missing		1			1		1				1	4
	No	76	55	130	29	9		45	186	61	3	95	689
Diabetes	Yes	20	16	36	7	7		4	12	8	2	20	132
	Missing		2	93			13	15	18				141
Family history of	No	90	42	165	35	16		54	192	67	5	102	726
ccRCC	Yes	5	4	22	1	0		1	6	2	0	3	43
	Missing	1	27	72			13	9	18			10	193
	Current smoker	23	21	66	9	4	6	11	52	18	1	28	239
Tobacco status	Ex-smoker	21	30	62	15	3	3	15	27	15	0	44	235
	Never	52	22	131	11	9	4	37	137	36	4	43	486
	Missing				1			1					2
	Mean	0.7	1.6	3.4		1.3	5.4	1.3	1.5	1.3	2.2	3.3	2.2
PFOA (ng/mL)	(st. dev.)	(0.5)	(1.1)	(2.1)		(0.6)	(4.1)	(0.9)	(1.4)	(0.6)	(2.2)	(1.7)	(1.9)

Fig. 2

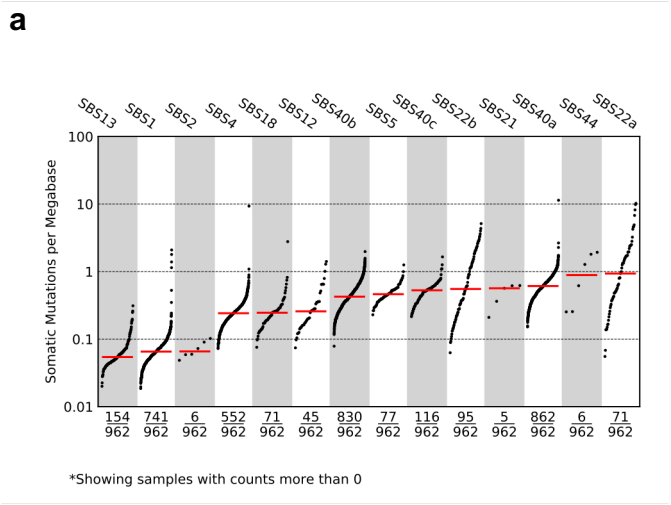
a
SBS13
SBS1
SBS2
SBS4
SBS18
SBS12
SBS40b
SBS5
SBS40c
SBS22b
SBS21
SBS40a
SBS44
SBS22a
Somatic Mutations per Megabase
100
10
1
0.1
0.01
154 962
741 962
6 962
552 962
71 962
45 962
830 962
77 962
116 962
95 962
5 962
862 962
6 962
71 962
*Showing samples with counts more than 0

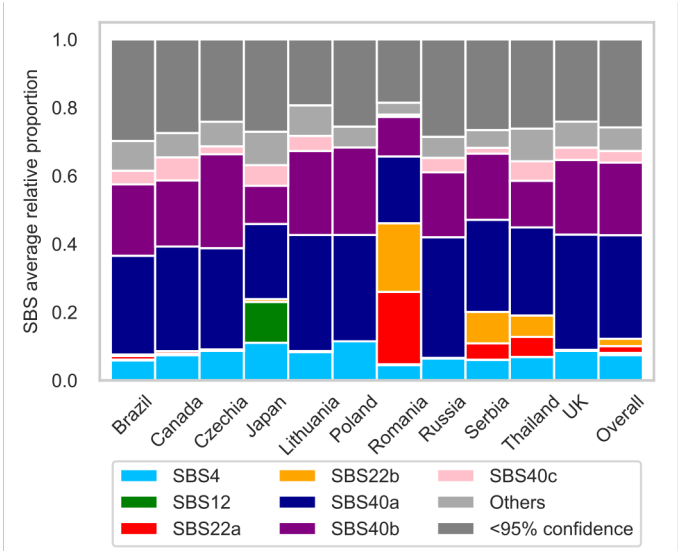
b
SBS average relative proportion
1.0
0.8
0.6
0.4
0.2
0.0
Brazil
Canada
Czechia
Japan
Lithuania
Poland
Romania
Russia
Serbia
Thailand
UK
Overall
SBS4
SBS12
SBS22a
SBS22b
SBS40a
SBS40b
SBS40c
Others
<95% confidence

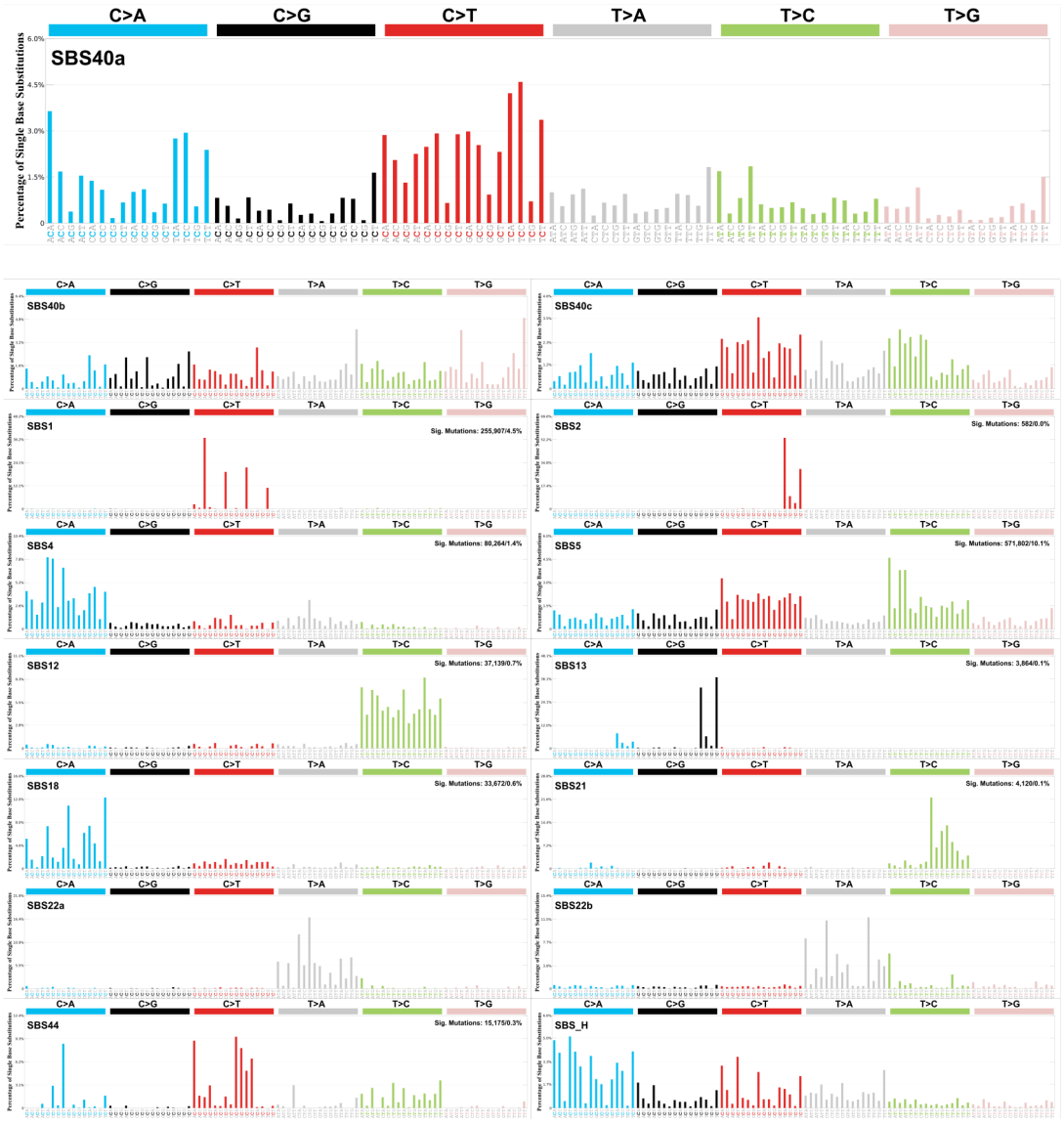
c
C>A
C>G
C>T
T>A
T>C
T>G
SBS40a
Percentage of Single Base Substitutions
SBS40b
SBS40c
SBS1
Sig. Mutations: 255,907/4.5%
SBS2
Sig. Mutations: 582/0.0%
SBS4
Sig. Mutations: 80,264/1.4%
SBS5
Sig. Mutations: 571,802/10.1%
SBS12
Sig. Mutations: 37,139/0.7%
SBS13
Sig. Mutations: 3,864/0.1%
SBS18
Sig. Mutations: 33,672/0.6%
SBS21
Sig. Mutations: 4,120/0.1%
SBS22a
SBS22b
SBS44
Sig. Mutations: 15,175/0.3%
SBS_H

Fig. 3

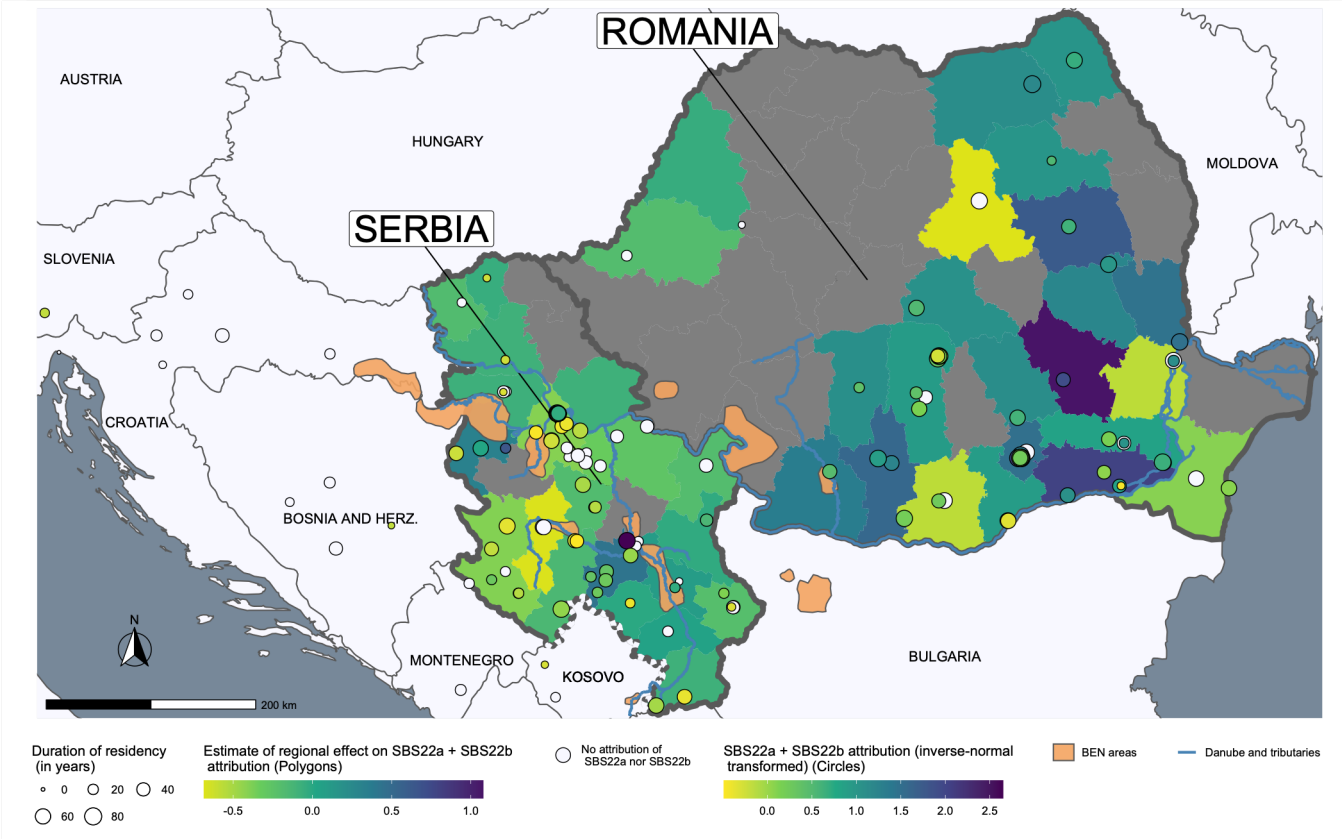
ROMANIA
SERBIA
AUSTRIA
HUNGARY
MOLDOVA
SLOVENIA
CROATIA
BOSNIA AND HERZ.
MONTENEGRO
KOSOVO
BULGARIA
N
200 km
Duration of residency (in years)
0
20
40
60
80
Estimate of regional effect on SBS22a + SBS22b attribution (Polygons)
-0.5
0.0
0.5
1.0
No attribution of SBS22a nor SBS22b
SBS22a + SBS22b attribution (inverse-normal transformed) (Circles)
0.0
0.5
1.0
1.5
2.0
2.5
BEN areas
Danube and tributaries

Fig. 4

a

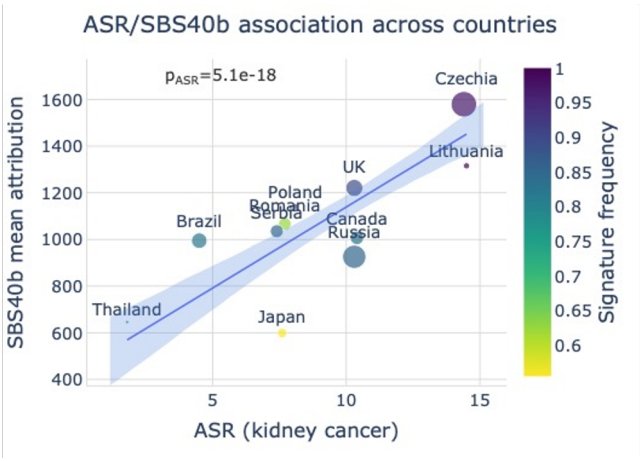
ASR/SBS40b association across countries
pASR=5.1e-18
SBS40b mean attribution
ASR (kidney cancer)
Signature frequency
Czechia
Lithuania
UK
Poland
Romania
Serbia
Brazil
Canada
Russia
Thailand
Japan

b

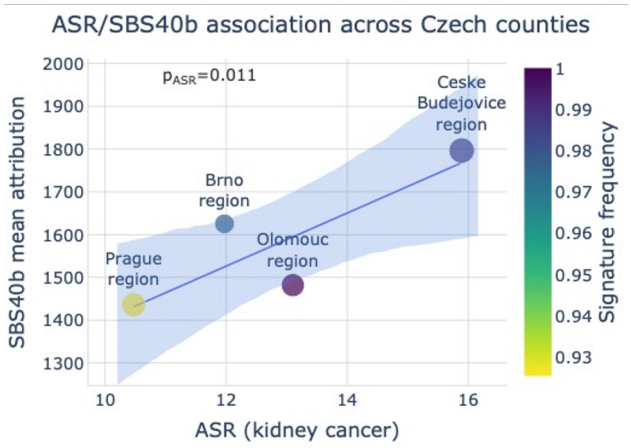
ASR/SBS40b association across Czech counties
pASR=0.011
SBS40b mean attribution
ASR (kidney cancer)
Signature frequency
Ceske Budejovice region
Brno region
Olomouc region
Prague region

c

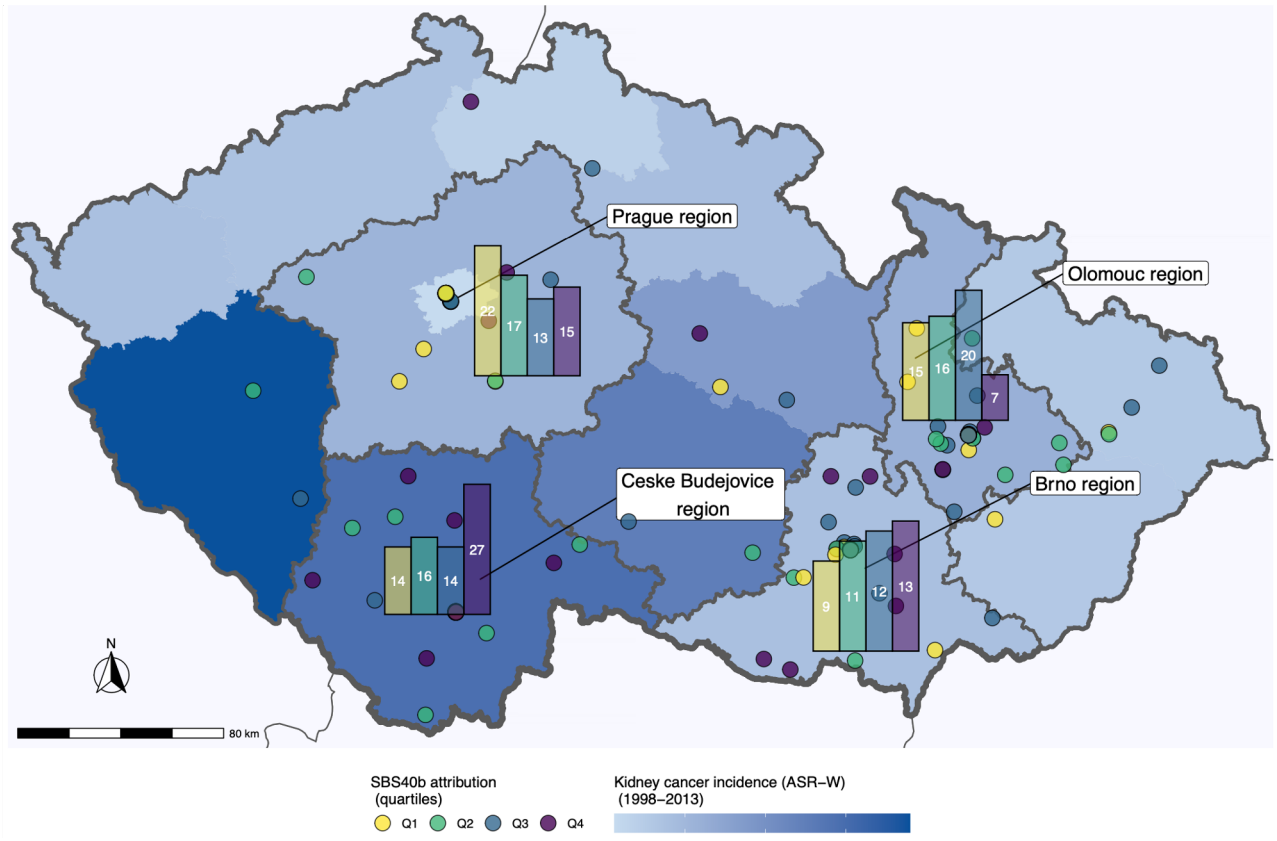
Prague region
Olomouc region
Ceske Budejovice region
Brno region
22
17
13
15
15
16
20
7
14
16
14
27
9
11
12
13
N
80 km
SBS40b attribution (quartiles)
Q1
Q2
Q3
Q4
Kidney cancer incidence (ASR–W) (1998–2013)

Fig. 5

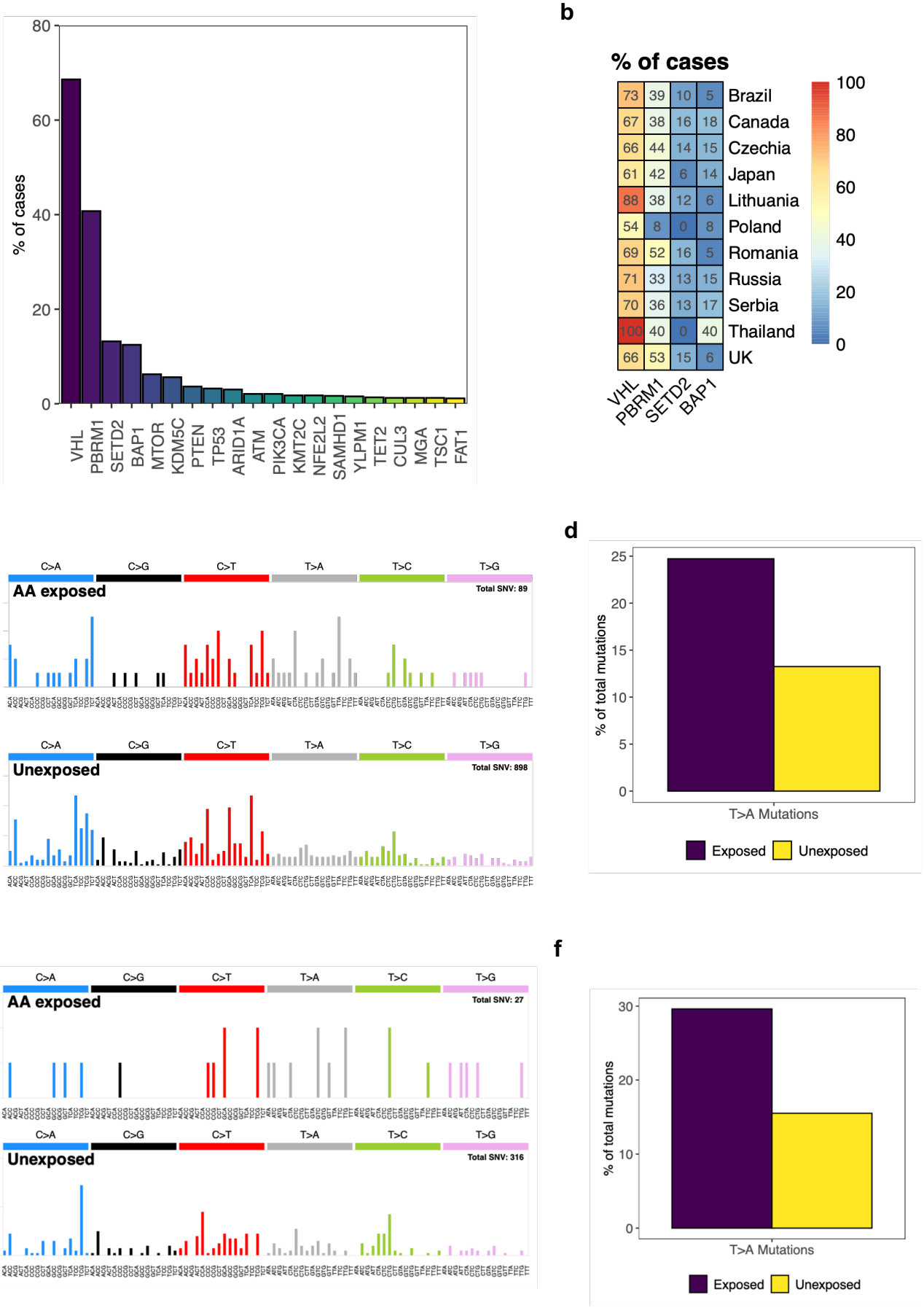
a
% of cases
VHL
PBRM1
SETD2
BAP1
MTOR
KDM5C
PTEN
TP53
ARID1A
ATM
PIK3CA
KMT2C
NFE2L2
SAMHD1
YLPM1
TET2
CUL3
MGA
TSC1
FAT1
b
% of cases
Brazil 73 39 10 5
Canada 67 38 16 18
Czechia 66 44 14 15
Japan 61 42 6 14
Lithuania 88 38 12 6
Poland 54 8 0 8
Romania 69 52 16 5
Russia 71 33 13 15
Serbia 70 36 13 17
Thailand 100 40 0 40
UK 66 53 15 6
VHL PBRM1 SETD2 BAP1
c
C>A C>G C>T T>A T>C T>G
AA exposed
Total SNV: 89
Mutation Count
Unexposed
Total SNV: 898
d
% of total mutations
T>A Mutations
Exposed
Unexposed
e
AA exposed
Total SNV: 27
Unexposed
Total SNV: 316
f
% of total mutations
T>A Mutations
Exposed
Unexposed

Extended Data Fig. 1.

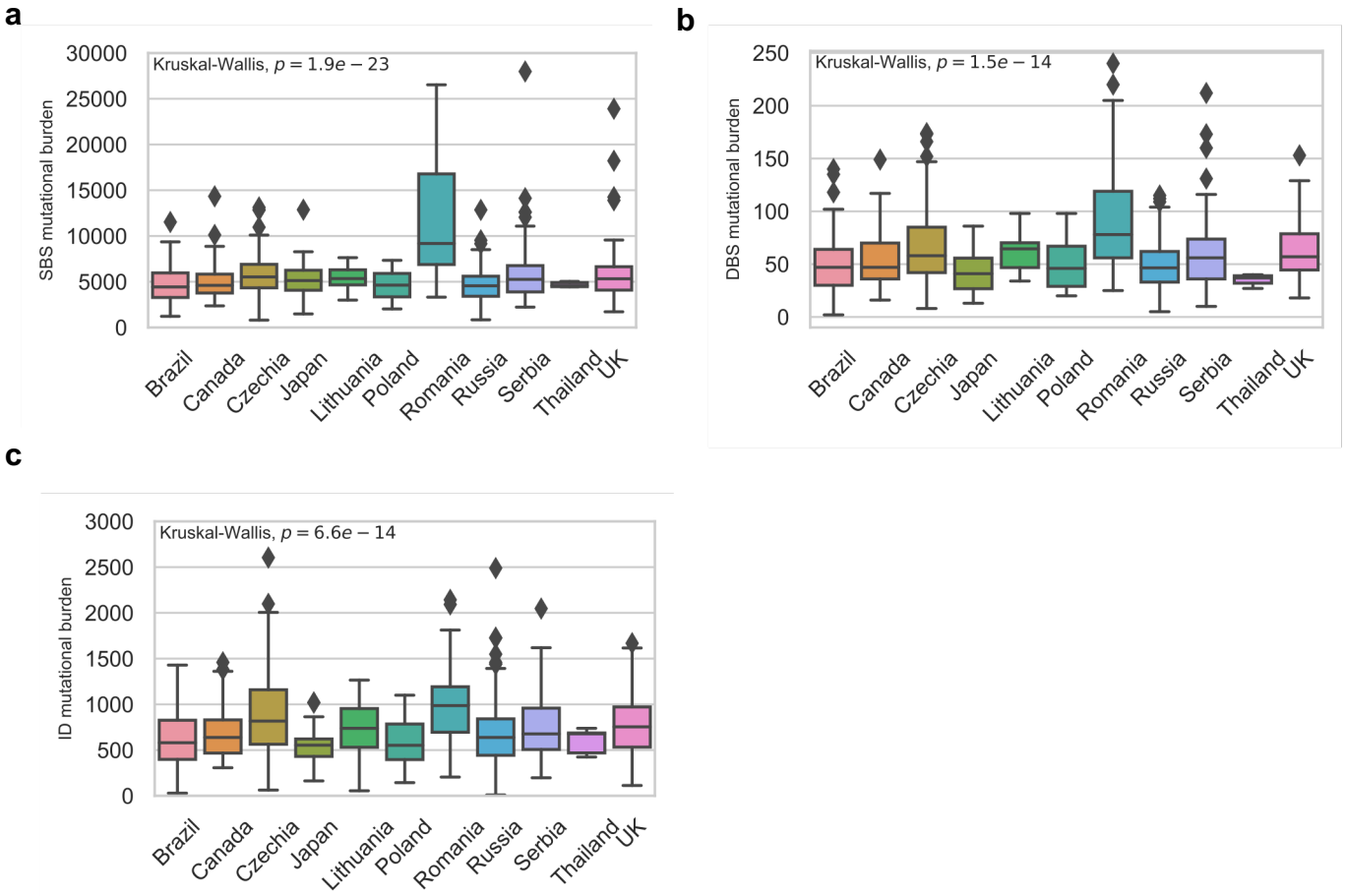

Extended Data Fig. 2.

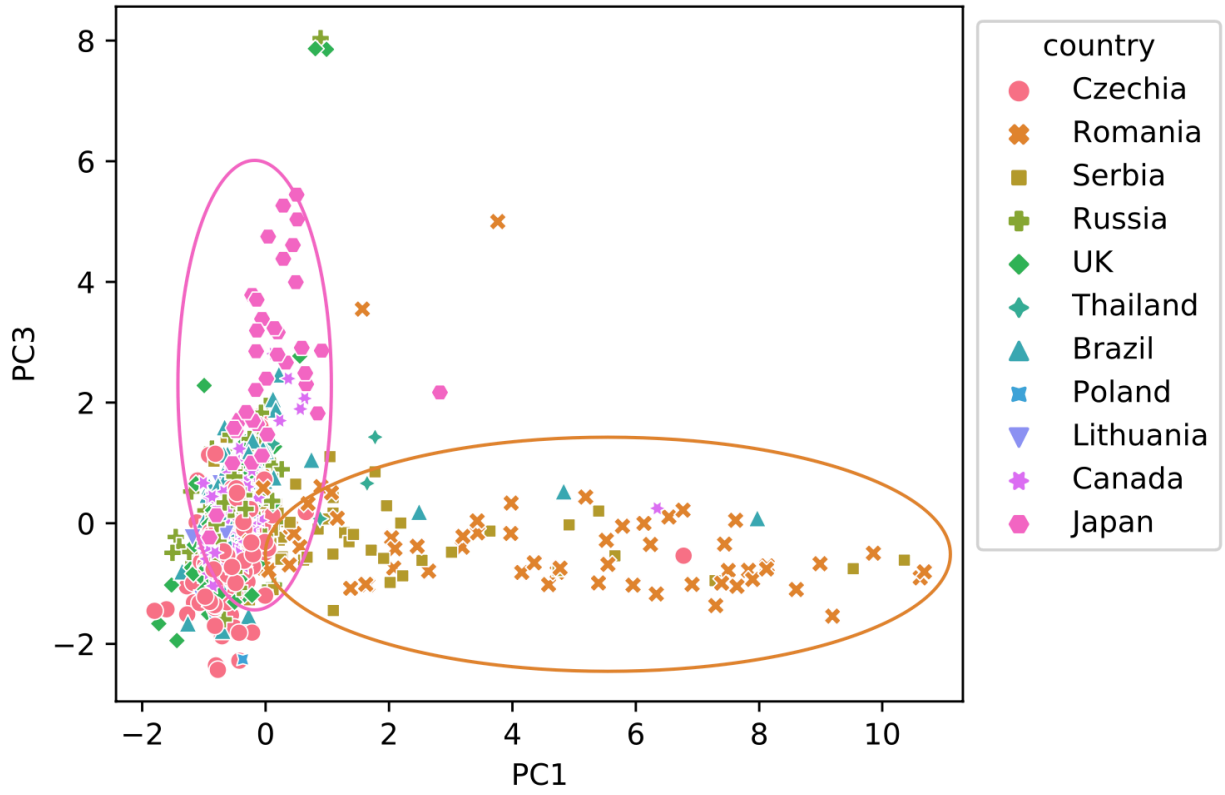

Extended Data Fig. 3.

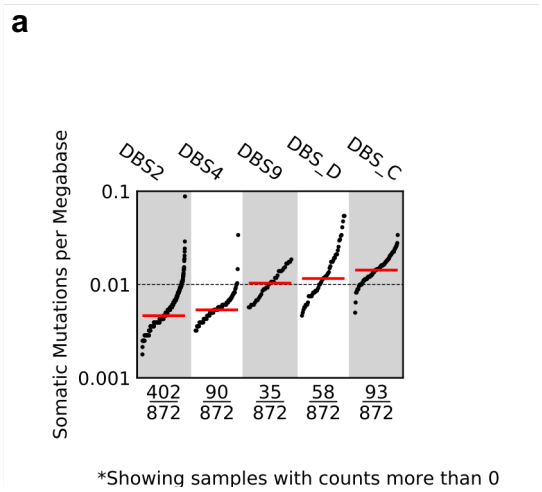

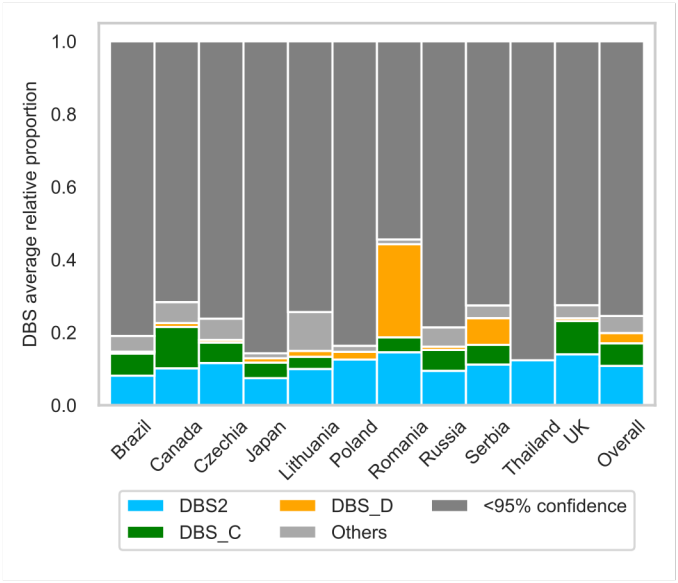

c

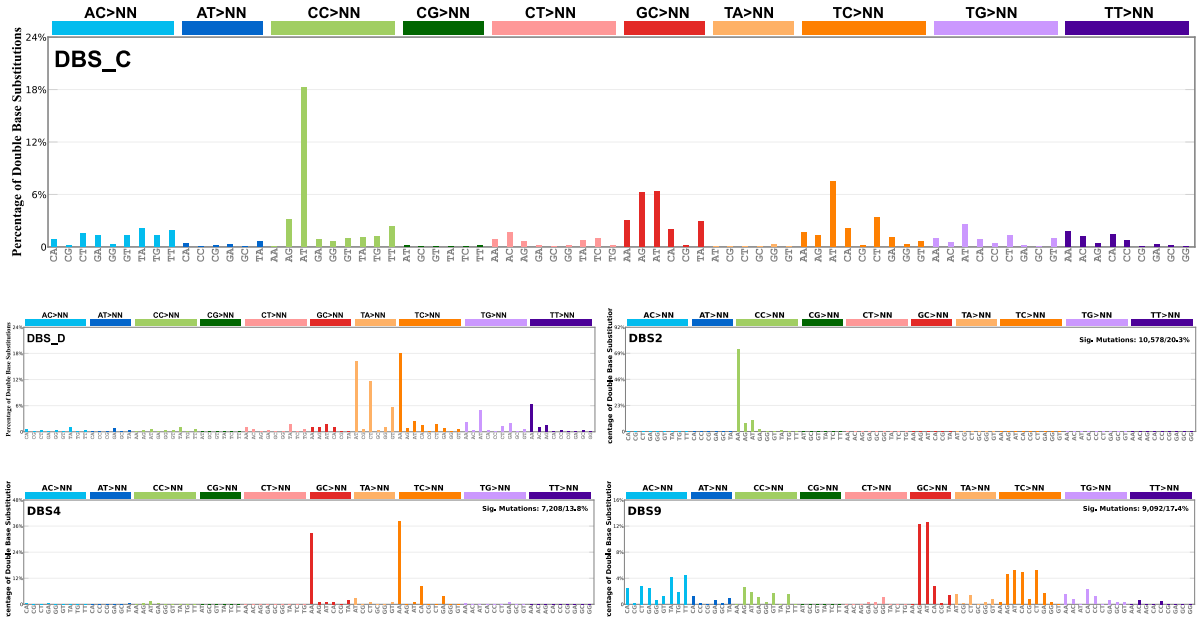

Extended Data Fig. 4.

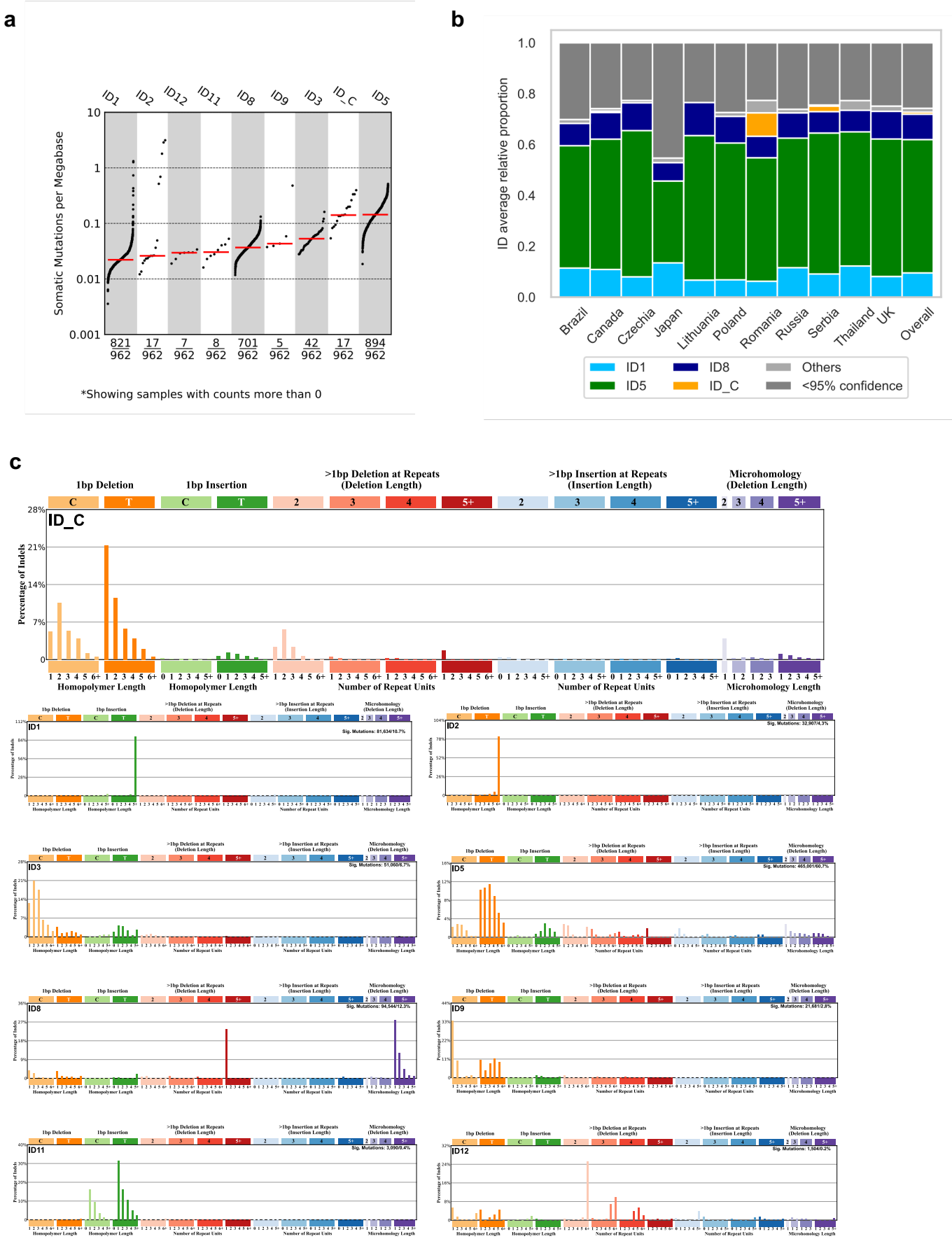

Extended Data Fig. 5.

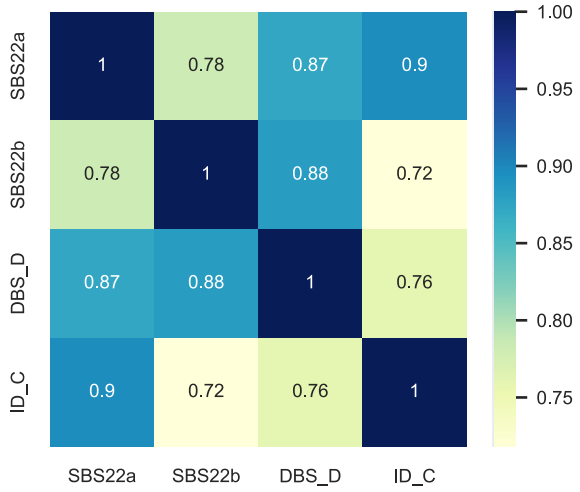

Extended Data Table 1.

Country	N cases	SBS22a (%)	SBS22b (%)	DBS_D (%)	ID_C (%)	SBS22a or SBS22b (%)	Any (%)
Romania	64	45 (70.3)	48 (75.0)	42 (65.6)	13 (20.3)	53 (82.8)	54 (84.4)
Serbia	69	16 (23.2)	33 (47.8)	11 (15.9)	3 (4.3)	35 (50.7)	36 (52.2)
Thailand	5	3 (60.0)	3 (60.0)	0 (0.0)	0 (0.0)	4 (80.0)	4 (80.0)
Brazil	96	3 (3.1)	3 (3.1)	1 (1.0)	0 (0.0)	3 (3.1)	3 (3.1)
Canada	73	2 (2.7)	0 (0.0)	2 (2.7)	1 (1.4)	2 (2.7)	3 (4.1)
Czechia	259	1 (0.4)	5 (1.9)	32 (12.4)	0 (0.0)	6 (2.3)	37 (14.3)
UK	115	1 (0.9)	0 (0.0)	31 (27.0)	0 (0.0)	1 (0.9)	31 (27.0)
Russia	216	0 (0.0)	1 (0.5)	26 (12.0)	0 (0.0)	1 (0.5)	27 (12.5)
Poland	13	0 (0.0)	0 (0.0)	1 (7.7)	0 (0.0)	0 (0.0)	1 (7.7)
Lithuania	16	0 (0.0)	1 (6.2)	1 (6.2)	0 (0.0)	1 (6.2)	2 (12.5)
Japan	36	0 (0.0)	1 (2.8)	1 (2.8)	0 (0.0)	1 (2.8)	1 (2.8)

Extended Data Fig. 6.

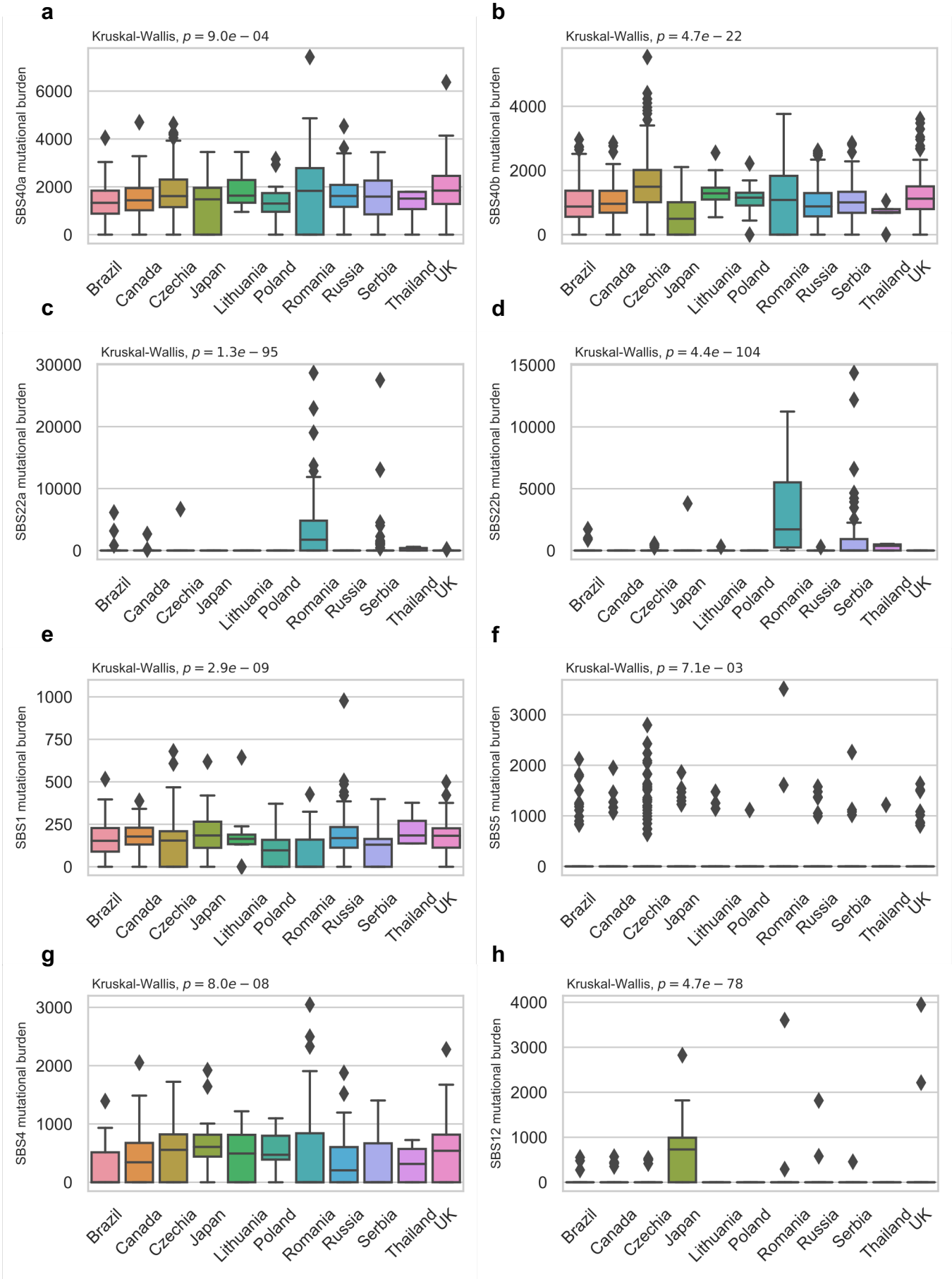

Extended Data Fig. 7.

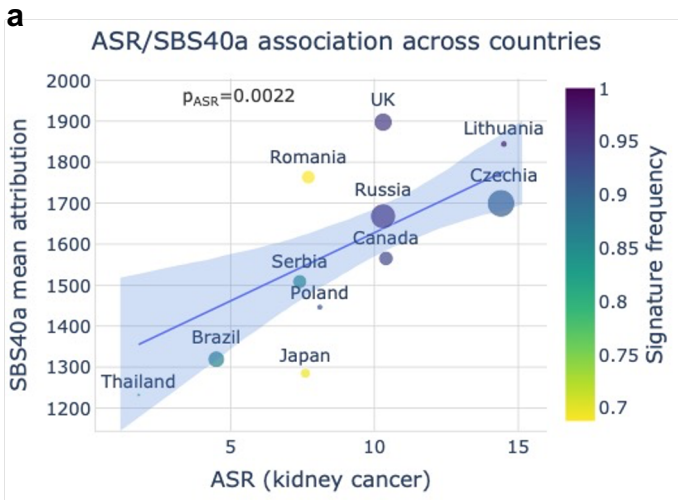

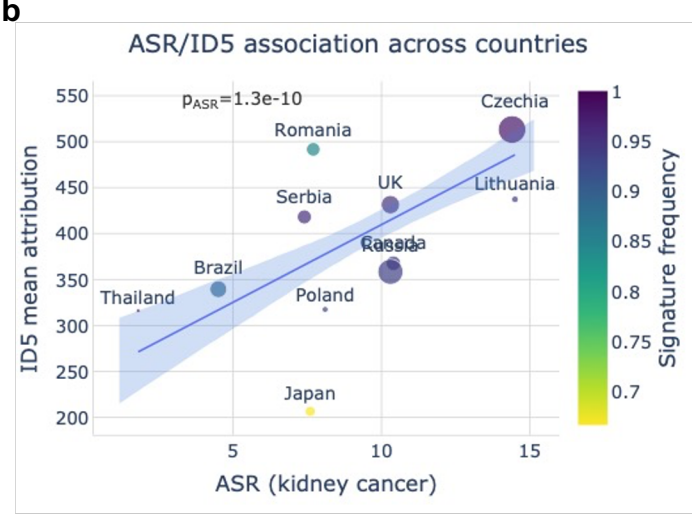

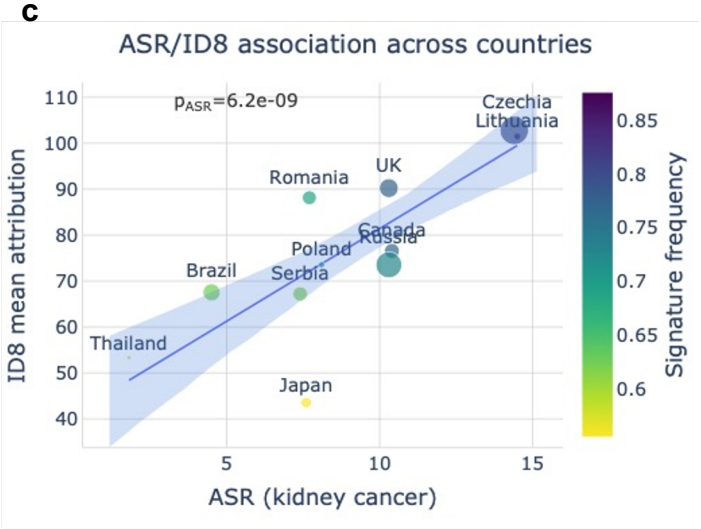

Extended Data Fig. 8.

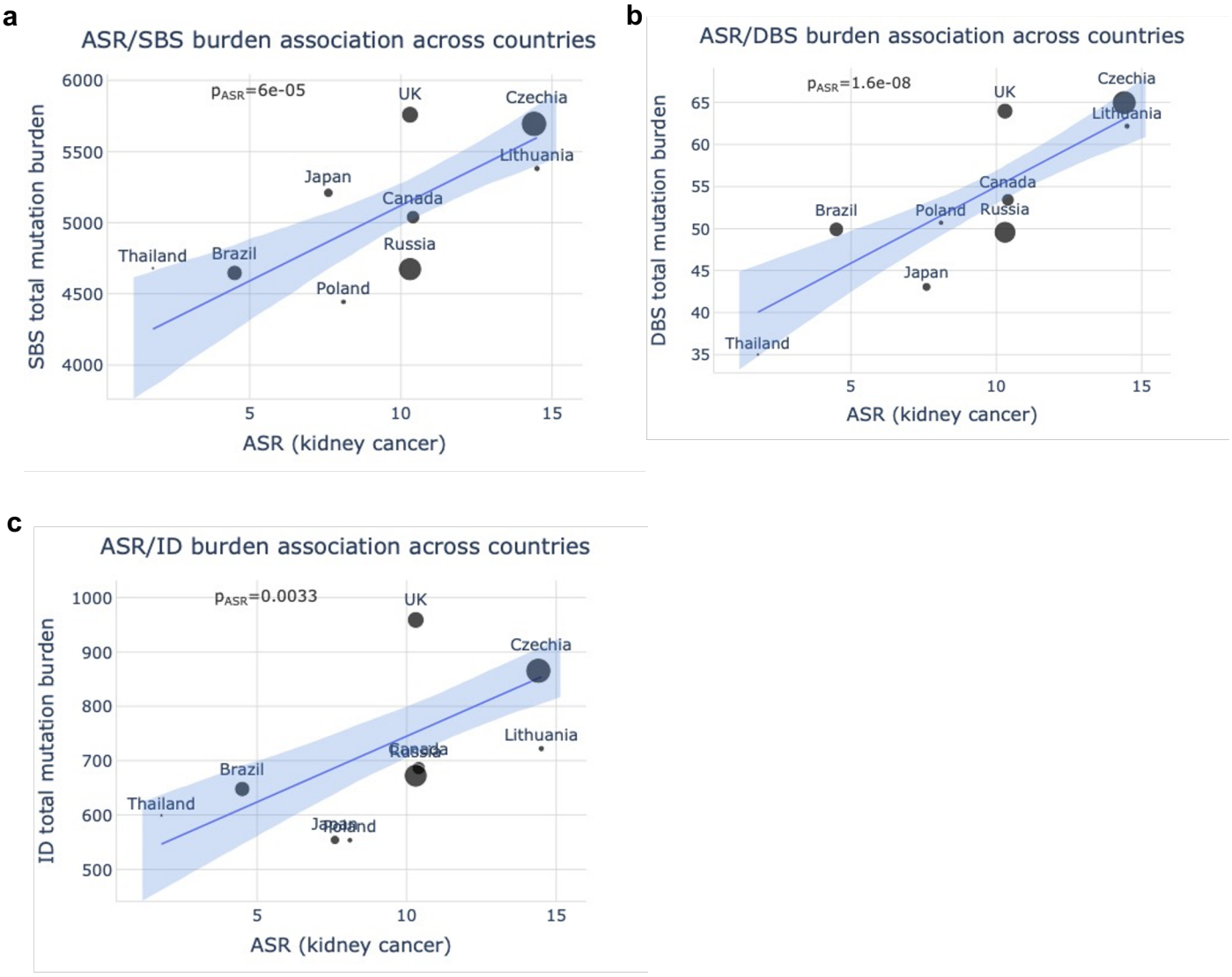

Extended Data Fig. 9.